Biomarkers reveal two paramount Pliocene-Pleistocene connectivity events in the Caspian Sea Basin

Iuliana Vasiliev [a,*], Marcel T.J. van der Meer [b], Marius Stoica [c], Wout Krijgsman [d], Gert-Jan Reichart [b,d], Sergei Lazarev [e,f], Geanina A. Butiseacă [a,g], Eva M. Niedermeyer [a], Elmira Aliyeva [h], Christian G.C. van Baak [i], Andreas Mulch [a,g]

[a] *Senckenberg Biodiversity and Climate Research Centre (SBiK-F), Senckenberganlage 25, D-60325 Frankfurt am Main, Germany*
[b] *Royal Netherlands Institute of Sea Research, P.O. Box 59, 1790 AB Den Burg, Texel, the Netherlands*
[c] *Department of Geology and Geophysics, Bucharest University, Nicolae Balcescu 1, 010041 Bucharest, Romania*
[d] *Department of Earth Sciences, Utrecht University, Princetonlaan 8A, 3584 CB Utrecht, the Netherlands*
[e] *Department of Geosciences, University of Fribourg, Chemin du Musée 6, 1700 Fribourg, Switzerland*
[f] *JURASSICA Museum, Route de Fontenais, 21, 2900 Porrentruy, Switzerland*
[g] *Institute of Geosciences, Goethe University Frankfurt, Altenhöferallee 1, 60438 Frankfurt am Main, Germany*
[h] *Geological Institute of Azerbaijan, H. Javid Av. 29A, AZ1143 Baku, Azerbaijan*
[i] *CASP, West Building, Madingley Rise, Madingley Road, CB3 0UD Cambridge, United Kingdom*

A R T I C L E   I N F O

A B S T R A C T

Landlocked basins like the Caspian Sea are highly sensitive to changes in their hydrological budget, especially at times of disconnection from the global ocean. Here, we reconstruct the Pliocene to Pleistocene palaeohydrological and palaeoenvironmental changes occurring in the South Caspian Basin between ~3.6 and ~ 1.9 Ma, using compound-specific hydrogen isotope (δ^2H) data on long chain n-alkanes and alkenones. Additionally, we established a record of mean annual air temperature (MAT) and the source of organic matter, based on the relative distribution of branched and isoprenoid glycerol dialkyl glycerol tetraethers (BIT). The ~55‰ variation in the δ^2H measured on the terrestrial plant long chain n-alkanes indicates significant continental hydrological changes in the region surrounding the Caspian Sea over the investigated 1.7 Myr interval. The MAT and BIT data show that the so-called Akchagylian marine incursion at around 2.75 Ma, marked by influx of marine biota into the Caspian Basin, originated from a cold region of the open ocean, endorsing a hydrological connection with the Arctic domain. The onset of the regional Apsheronian stage at ~2.13 Ma, identified by the invasion of *Tyrrhenocythere* sp. ostracods, coincided with a change towards constant δ^2H$_{n-alkane}$ and is shortly followed by the occurrence of alkenones in the Caspian Basin. The relative distributions of alkenones and their δ^2H values indicate that a connection with a saline basin, most likely the Black Sea, was established at the Akchagylian–Apsheronian transition.

1. Introduction

Landlocked lacustrine basins like the Caspian Sea are extremely sensitive to changes in their overall hydrological budget. Water-level changes directly reflect modifications in river runoff, evaporation and precipitation while connections to open marine basins completely change the environmental conditions of the basin, causing major faunal turnovers (Krijgsman et al., 2019 and references therein). Because of its intracontinental geographical position, the Caspian Basin is of key importance for water vapour recycling and eastward transport of

moisture over Central Asia (e.g., Dong et al., 2018). Therefore, modifications to the areal extent of the Caspian Sea will inevitably change its evaporation potential and hence directly affect warm season precipitation in today's arid parts of Central Asia. At current, the Caspian Basin represents a vast reservoir of anomalohaline (i.e., brackish) water. It is highly sensitive to palaeohydrological and paleoenvironmental changes over its 3.5 million km^2 - wide catchment area, which extends northward to the central part of the East European Plain (Panin, 2005; Zonn et al., 2010). The Caspian catchment stretches over regions covered by forests and steppes in the Volga and Ural valleys and mountainous

---

forests and arid regions in the Caucasus and Transcaspian areas (Fig. 1). The Caspian Basin became isolated from the Black Sea at the Mio-Pliocene transition, when a major drop in water level resulted in progradation of Volga deltaic deposits that reached the South Caspian Basin (Clauer et al., 2000; Vincent et al., 2010; van Baak et al., 2019, Fig. 2). Since then, the Caspian Basin has experienced numerous transgressional cycles with water level fluctuating tens to hundreds of meters resulting in enormous lateral shore line changes, especially in the topographically subdued northern part of the basin (Yanina, 2013; Yanchilina et al., 2019).

Here, we reconstruct palaeohydrological and palaeoenvironmental changes in the Caspian Basin (Fig. 1), using compound-specific hydrogen isotope (δ^2H) data on excellently preserved biomarkers, long chain n-alkanes and alkenones extracted from the Pliocene to Pleistocene successions exposed along the Lokbatan section. Long chain n-alkanes originate from higher plant waxes growing in the lake surroundings or transported by rivers feeding the lake basin and their hydrogen isotope ratios (δ^2H$_{n\text{-alkanes}}$) reflect hydrological changes during plant growth in these environments (e.g., Sachse et al., 2012). δ^2H values of n-alkanes have been shown to reflect primarily the hydrogen isotope composition of precipitation (δ^2H$_{precip}$) (e.g., Sachse et al., 2012) and are influenced to a variable degree by evapotranspiration (e.g., Sachse et al., 2006). δ^2H$_{n\text{-alkanes}}$ data have been successfully used in reconstruction of terrestrial paleo-δ^2H$_{precipitation}$ and δ^2H$_{paleo\text{-evaporation}}$ (e.g., Sachse et al., 2004; Schefuss et al., 2005; Niedermeyer et al., 2016; Feakins et al., 2020) bearing in mind plant-physiology-induced limitations to the quantitative interpretation of the δ^2H$_{precipitation}$. In contrast, long chain alkenones are derived from haptophyte algae within the basin water column and their δ^2H values (δ^2H$_{alkenones}$) typically reflect changes in the hydrogen isotope composition of Caspian Sea water (e.g., Schwab and Sachs, 2011). Combined δ^2H$_{n\text{-alkanes}}$ and δ^2H$_{alkenones}$ data allow identifying the relative changes in received precipitation source versus input of different waters into the Caspian Basin.

We focus on hydrological changes that occur first at the lower part of the Akchagylian (~2.95 Ma) and afterwards at the base of the Apsheronian regional stages (ca. ~2.13 Ma) to elucidate relationships between marine connectivity events and faunal turnovers. To frame these hydrological changes, we present mean annual air temperature (MAT') data based on the relative distributions of branched glycerol dialkyl glycerol tetraether (brGDGTs) lipids primarily derived from soil bacteria (e.g., Weijers et al., 2007a; Peterse et al., 2012). The brGDGT lipid record further serves for the reconstruction of paleo-soil pH within the catchment of the rivers transporting the brGDGTs into the Caspian Basin. We further quantify the so-called branched and isoprenoid tetraether (BIT) index (Hopmans et al., 2004) that compares the amount of brGDGTs to crenarchaeol (isoprenoidal GDGTs) to determine the relative contribution of aquatically produced versus soil-derived organic matter. We ultimately integrate these paleoclimatic and paleoenvironmental data into the most advanced age model for sedimentation in the Caspian Basin (Lazarev et al., 2021) resulting from extensive magnetostratigraphic and radiometric dating over the past decade (van Baak et al., 2013; Forte et al., 2015; Richards et al., 2018; Hoyle et al., 2020; Lazarev et al., 2019). Collectively our biomarker, sedimentological and chronometric data show two distinct phases of connectivity to two completely different water masses within the 1.7 million years time interval studied here. This is the first documentation of biomarkers-based proxy records in the sedimentary succession of the Caspian Basin, which opens up new possibilities for improved palaeoenvironmental reconstructions through geological time of this crucial region of Central Eurasia.

2. Stratigraphy of sampled interval and age model

The Lokbatan section (base section: N 40°20′3.96″, E 49°44′58.28″) is located 12 km west of the present-day Caspian coastline, south of the city of Baku (Azerbaijan) (Fig. 1). The section comprises the uppermost part of the Productive Series (Surakhany Suite) and the overlying Akchagylian and Apsheronian (Fig. 2; Hinds et al., 2004 Vincent et al., 2010; van Baak et al., 2013). The 520-m-thick Productive Series is characterised by an alternation of predominantly grey, green and reddish-brown silty clays and (sub-) meter-scale friable sandstone layers. The Surakhany Suite of the Productive Series has previously been interpreted as an ephemeral fluvial flood plain, overbank pond and saline lake facies (Vincent et al., 2010; Richards et al., 2021). At 520 m, an abrupt lithological change to grey clays and silts marks the Akchagylian transgression, recently dated in Lokbatan at 2.95 ± 0.02 Ma (Lazarev
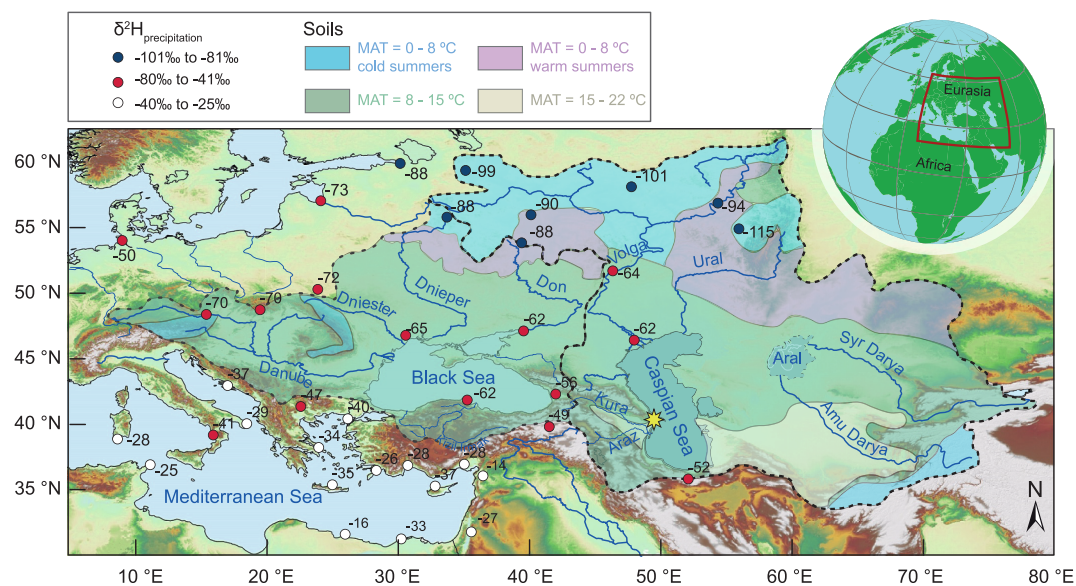

Fig. 1. Map of showing the drainage basin of the Black and Caspian Seas as remnants of the former Paratethys domain. Major rivers draining into the Paratethys are indicated. The values of the present day precipitation δ^2H are reported according to IAEA (2019). Long-term means were calculated by selecting yearly means in which isotope content have been measured at least in 75% of the precipitation for that year and at least over eight months (IAEA, 2019). Soil temperatures in the larger Paratethys domain drainage basin are indicated. Remark that the lager Paratethys extent would have collected rivers feeding, next to the Caspian Sea, also the Black Sea and Aral Lake. The star locates the Lokbatan section.
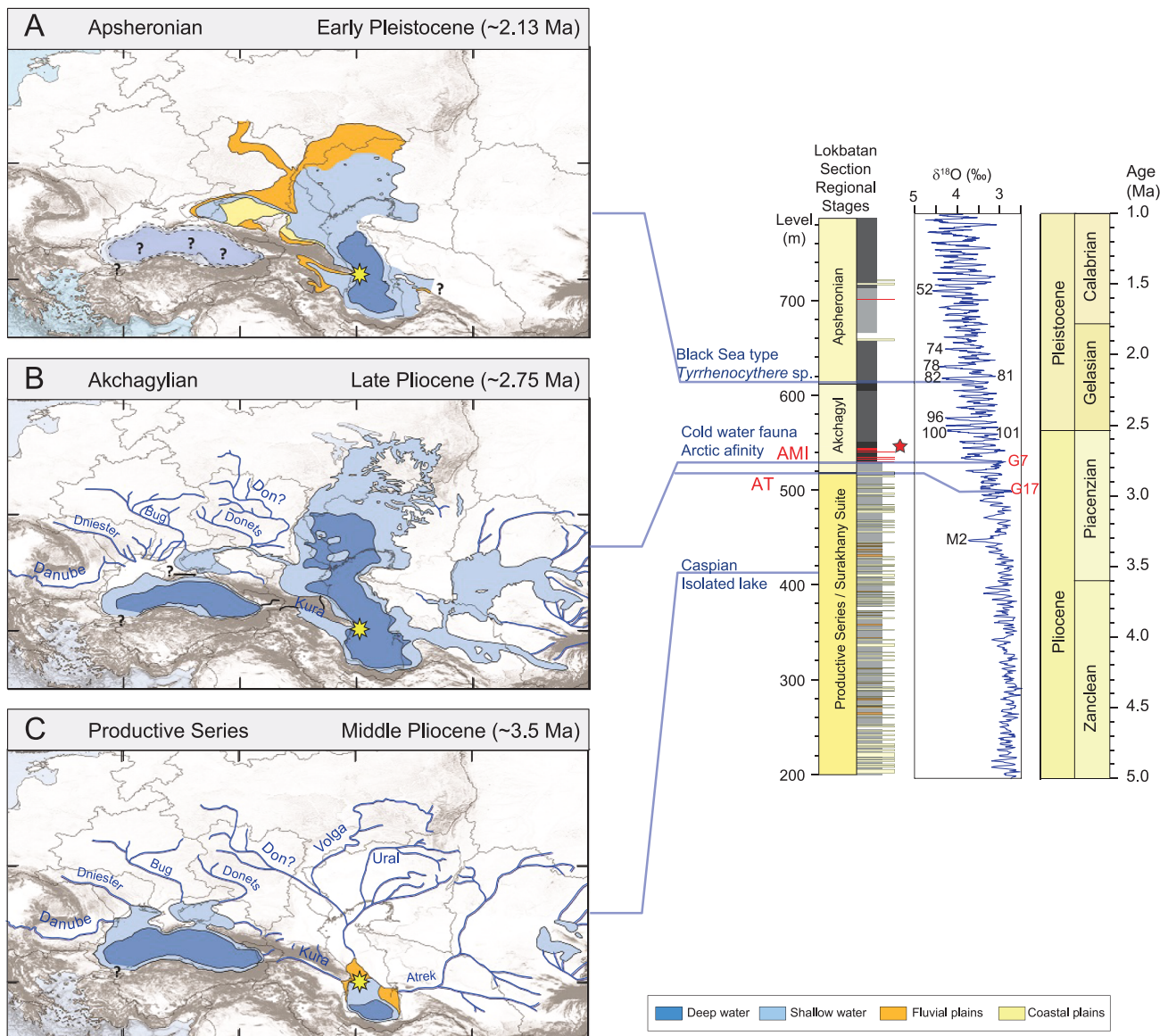
Fig. 2. Extent of Paratethys at different time-slices. A) During Apsheronian, between 2.13 and 0.84 Ma Caspian was a smaller lake-sea; B) Between 2.95 and 2.13 Ma the Caspian was a very large lake-sea and; C) During the deposition of the Productive series (~5 to 2.95 Ma), the Caspian was a small lake; The schematic stratigraphic log of Lokbatan section with the regional stages correlated to the global stratigraphic scheme and δ18O curve of Lisiecki and Raymo (2005). The yellow star indicates the location of Lokbatan section. Observe that some rivers (i.e., Don) may have been feeding different Paratethys sub-basins at different times. The red start locates the multiple ash layers interval with an 40Ar/39Ar age of ~2.69 Ma (Hoyle et al., 2020). AT and AMI indicate Akchagylian transgression and Akchagylian marine incursion, respectively. (For interpretation of the references to colour in this figure legend, the reader is referred to the web version of this article.)

et al., 2021). The following interval 520–545 m contains numerous volcanic ash layers, nine of which were dated by 40Ar/39Ar geochronology with ages ranging from 2.60 ± 0.03 Ma to 2.73 ± 0.09 Ma (Hoyle et al., 2020). This interval pre-dates the Pliocene–Pleistocene transition (2.58 Ma) and could be correlated to the MIS G8–MIS 104 interval based on palynological records that showed a relationship with global δ18O stacks and the obliquity record (Hoyle et al., 2020). At 529 m an influx of marine species, widely known as the Akchagylian flooding or Akchagylian marine incursion was dated at 2.75 Ma (Fig. 3).Higher up, the section continues with ~110 m of fine bedded blue and black clays, (light-) grey silty clays and thin ferruginous layers. These clays are rich in molluscs (*Dreissena rostriformis*, cardiid bivalves) and ostracods. The section continues with ~50 m of grey clays and silty intercalations, capped by fine-grained pebbles and clays rich in mollusc shells. van Baak et al. (2013) placed the Akchagylian–Apsheronian boundary in the Lokbatan section at 660 m, based on the abundance of the ostracod

genus *Tyrrhenocythere*. More detailed ostracod analysis now shows that the first appearance of *Tyrrhenocythere* genus takes place at level 616.5 m of the Lokbatan section (Fig. 3). In other sections of the Kura Basin (Hajigabul and Goychay located eastern and central part of Azerbaijan respectively), the first occurrence of *Tyrrhenocythere azerbaijanica* was shown to closely correspond to the Akchagylian–Apsheronian boundary, and to correlate magnetostratigraphically with the Reunion subchron and an age of ~2.13 Ma (Lazarev et al., 2019). Consequently, we conclude that the base of the Apsheronian in the Lokbatan section should be re-assigned to 616.5 m instead of 660 m (Fig. 3). Finely-laminated brown-grey silty clays with thin ferruginous layers are typical for the lower part of the Apsheronian. At 700 m, a three cm-thick whitish tuff layers are interbedded. Just before the top of this part of the section, at 715 m, a sharp change in lithology marks a return to homogeneous blue clay. Above this are two beds of slumped layers with reworked tuff elements and shell-fragments. The sharp change to blue
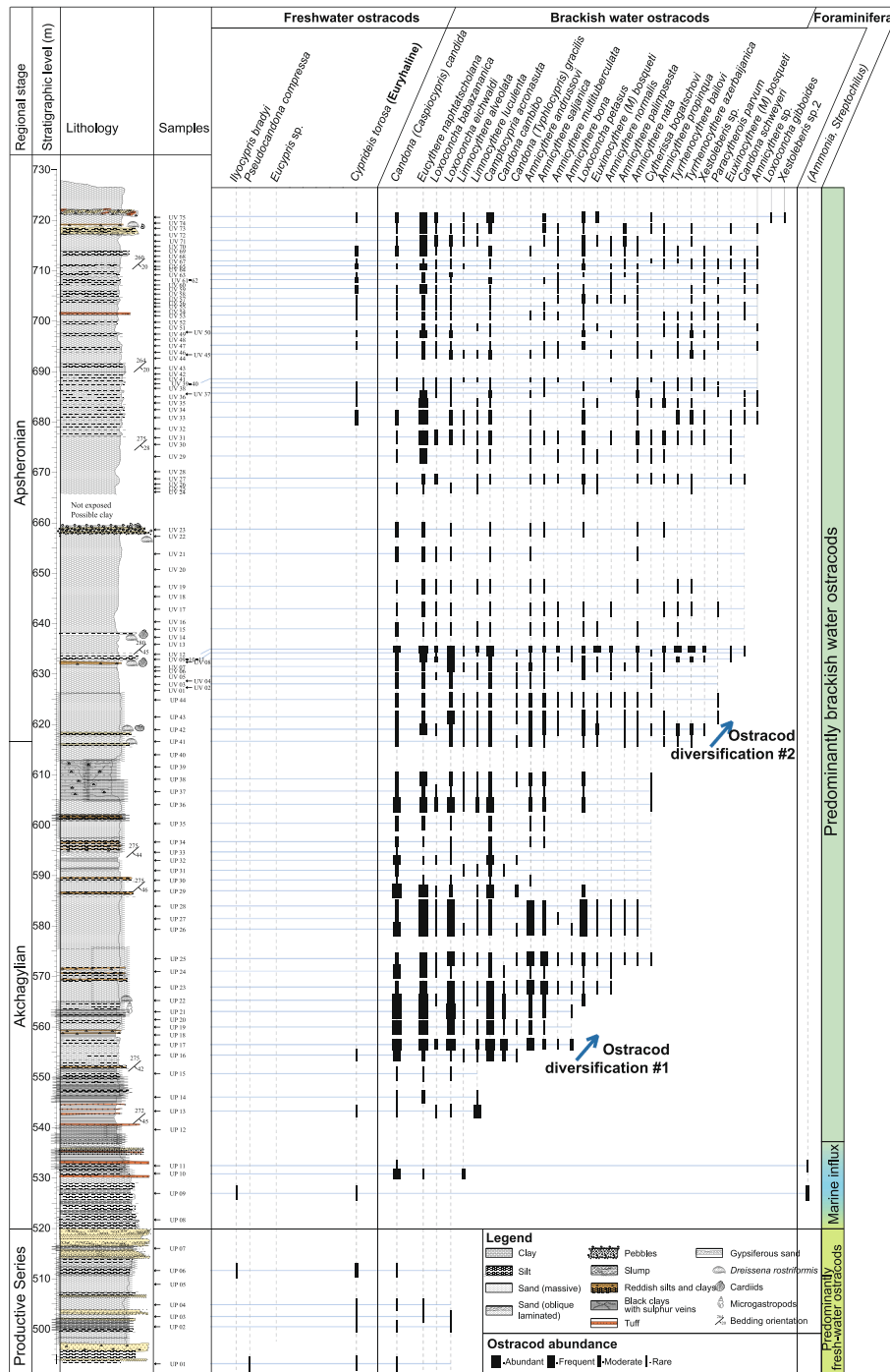
Fig. 3. Ostracod range chart for Lokbatan section. Remark the highlighted levels with foraminifera at the transition between Productive Series and Akchagylian and the steps in the ostracod diversification, the first one during Akchagylian and the second one at the Akchagylian–Apsheronian transition. Micropaleontology methods are as described in van Baak et al. (2013).

clays is also found 300 m further north (N 40°20′36.54″, E 49°44′20.54″), where the section continues. Upwards, the section consists of blue, dark-grey and brown clays with ferruginous layers and iron concretions (up to 40 cm in diameter).

The recent chronostratigraphic revision of the Akchagylian and Apsheronian successions in the Kura Basin (Lazarev et al., 2021) now allows us to calculate the ages of all sampled levels in the Lokbatan section, using linear interpolation of constant sedimentation rates between six age tie points with details provided in the Supplementary material.

3. Experimental and analytical methods

3.1. Lipid extraction, separation and analyses

Thirty-seven sedimentary rock samples weighing between 8 and 60 g were dried and thoroughly ground. To avoid possible contamination, which may have occurred during sampling and handling, the outer part of these samples was avoided during sub-sampling for lipid extraction. Larger samples (i.e., 10–60 g), were extracted using a Soxhlet apparatus with a dichloromethane – methanol (DCM/MeOH; 7.5:1, *v:v*) organic solvent mixture. Smaller samples (up to 15 g) were extracted by

accelerated solvent extraction (ASE, Dionex 200) using a DCM/MeOH (9:1, *v:v*) mixture at 100 °C and 1000 psi. All extracts were rotary – evaporated to near dryness and subsequently dried under a gentle N_2 flow. The total lipid extracts (TLE) were dried over an anhydrous Na_2SO_4 column. Elemental sulfur was removed using activated copper in DCM in the earlier obtained TLE. Copper flakes were activated with 2 M HCl and afterwards rinsed with MilliQ ultra-pure water, MeOH and DCM. This treatment was repeated up to four times when necessary. An aliquot of the desulfurized extract was separated using column chromatography with activated Al_2O_3 as stationary phase by subsequent elution with hexane/DCM (9:1, *v:v*), hexane/DCM (1:1, *v:v*), and a mixture of DCM/ MeOH (1:1, *v:v*) to obtain the apolar, ketone and polar fraction, respectively. *N*-alkanes were isolated from the apolar fraction using urea-adduction. The apolar fraction was dissolved in 200 μl MeOH/urea (~10%, H_2NCONH_2, Merck) solution. Next, 200 μl acetone and 200 μl hexane were added to the solution, frozen (−20 °C) and dried under N_2 flow. The straight (*n*-alkanes) compounds were captured during the formation of the urea crystals. These were washed with hexane to remove the non-adductable branched and cyclic compounds. Urea crystals, containing the adductable *n*-alkanes, were then dissolved in 500 μl MeOH and 500 μl MilliQ ultra-pure water mixture. The *n*-alkanes were subsequently extracted from the solution using hexane. The urea-adduction procedure was repeated up to three times to eliminate non-adductable compounds as much as possible. Alkenones were obtained from the ketone fraction using urea adduction as well using the earlier described procedure. All fractions were measured using Gas Chromatography/Flame Ionization Detector (GC/FID) first. The *n*-alkanes and alkenones were identified based on mass spectra using Gas Chromatography-Mass Spectrometry (GC–MS) on a Thermo-Finnigan Trace DSQ instrument. The fractions (dissolved in hexane) were injected on-column at 70 °C (CP-Sil 5CB fused silica column (30 m × 0.31 mm i.d, film thickness 0.1 μm). The oven program was set at constant pressure (100 kPa) and then programmed to increase to 130 °C at 20 °C min^{-1}, and then at 5 °C min^{-1} to 320 °C at which it was held isothermal for 10 min. Individual *n*-alkanes and alkenones were quantified by comparing to an internal standard and using a GC equipped with a flame ionization detector (FID). The polar fraction was concentrated under a N_2 gentle stream, dissolved in hexane/2-isopropanol (99:1, v:v) and filtered over a 0.4 μm PTFE filter prior to injection into an high performance liquid chromatography – atmospheric pressure chemical ionization/mass spectrometry (HPLC-MS).

3.2. Compound specific isotope analyses

3.2.1. Compound specific hydrogen isotope (δ^2H) analyses

Compound-specific hydrogen isotopes (δ^2H) of *n*-alkanes and alkenones were determined by gas chromatography-isotope ratio mass spectrometry (GC-TC-irMS) at the Organic Geochemistry Laboratories at Utrecht University and the Netherlands Institute of Sea Research (NIOZ). The δ^2H values of individual *n*-alkanes and alkenones were measured on the adducted *n*-alkane and alkenone fractions on a HP 6890 N Gas Chromatograph (GC) coupled to a Thermo-Finnigan Delta Plus XP Isotope Ratio Mass Spectrometer (irMS). The fractions (dissolved in hexane) were injected on-column at 70 °C, the oven being programmed to increase to 130 °C at 20 °C min^{-1}, and then at 5 °C min^{-1} to 320 °C at which it was held isothermal for 10 min. The film thickness of the CP-Sil 5 column was 0.4 μm and a constant flow of He was used at 1.5 ml min^{-1}. The compounds of the adducted *n*-alkane and alkenone fractions were pyrolyzed in an empty ceramic tube heated at 1450 °C which was pre-activated by a 5 min methane flow of 0.5 ml min^{-1}. H_3+ factors were determined daily on the isotope mass spectrometer and were at any time < 5. Each extract was measured between two and ten times. The large number of multiple analyses is related to the unusual results, which needed verification. H_2 gas with known isotopic composition was used as reference and a mixture of C_{16}–C_{32} *n*-alkanes with known isotopic composition (ranging from −42‰ to −256‰ vs. Vienna Standard

Mean Ocean Water (V-SMOW)) was used to monitor the performance of the system (Schimmelman Mixture A and B, Biogeochemical Laboratories, Indiana University). A squalane standard was co-injected with every sample and its average value was −171 ± 3‰, which compared favorably with its offline determined value of −168.9‰.

3.2.2. Compound specific carbon ($\delta^{13}C$) isotope analyses

The carbon isotope ratios ($\delta^{13}C$) of individual *n*-alkanes were measured on the adducted apolar fractions on the GC-C-irMS using similar conditions as for δ^2H measurements. The $\delta^{13}C$ values, expressed relative to the V-PDB standard, were calculated by comparison to a CO_2 reference gas (calibrated against NBS-19). Standard deviations were determined using a co-injected standard and attained ±0.3‰.

3.3. HPLC-MS analysis

3.3.1. HPLC-MS instrumentation

The polar fractions were measured at the Organic Geochemistry Laboratory of Utrecht University (UU) and the Senckenberg Biodiversity and Climate Research Centre (SBiK-F) following equal purification steps and similar instrumental conditions. The polar fraction was concentrated, dissolved in *n*-hexane/2-isopropanol (99:1, *v:v*), and filtered over a 0.4 μm PTFE filter prior to injection into a high performance liquid chromatography – atmospheric pressure chemical ionization/mass spectrometry (HPLC-MS). Analyses were performed using an Agilent 1290 Infinity series, 6130 Quadrupole UHPLC/MS equipped with auto-injector and Chemstation chromatography manager software. 10 μL of each polar fraction was injected and separation was achieved on an analytical Alltech Prevail Cyano column by elution with 90% *n*-hexane and 10% 9:1 (*v:v*) *n*-hexane:2-propanol. Conditions for the Agilent 1290 series were as follows: drying gas flow was set to 6.0 L × min^{-1} with a temperature of 200 °C, a nebulizer pressure of 25 psi, a vaporizer temperature of 400 °C, a capillary voltage of −3.5 kV and a corona current of 5 μA. Isoprenoidal and branched GDGT lipids were detected by scanning for their $[M + H]^+$ ion in selected ion monitoring (SIM) mode. At some levels we verified results by repeating runs. Additionally, the measurements at both UU and SBiK-F were giving equal results. We achieved an excellent separation of the peaks (Fig. 4). The chemical structures of the GDGTs and their $[M + H]^+$ are illustrated in Supplementary material.

3.3.2. Mean annual temperature and input of soil organic matter

Here, estimates of continental mean annual air temperature (MAT) are based on the relative distribution of brGDGT membrane lipids. The distribution of brGDGTs, expressed as the Methylation index of Branched Tetraethers (MBT) and the Cyclisation ratio of Branched Tetraethers (CBT) displays a significant linear correlation with modern MAT in the range of −6 to 27 °C (Weijers et al., 2007a). This method has been frequently used for continental MAT reconstructions in the geological past (e.g., Weijers et al., 2007b; Inglis et al., 2017; Miller et al., 2018). As rivers transport these membrane lipids to the oceans, analysis of marine sedimentary deposits close to the outflows of large rivers may provide high-resolution records of catchment-wide integrated continental temperature (Weijers et al., 2007a). The initial definition of MAT and pH proxies was subject to subsequent recalibration and refinement (e.g., Peterse et al., 2012; De Jonge et al., 2014).

From the multiple existing calibrations, we rely on Peterse et al. (2012) as a more conservative choice given that the expected environmental changes for the more than 1.7 Myr duration of the studied interval are large. Therefore, mean annual air temperature (MAT) and pH were estimated as follows (Peterse et al., 2012):

$$MAT' = 0.81 - 5.67*CBT + 31.0*MBT'$$

$$pH = 7.90 - 1.97*CBT$$

MBT' and CBT were calculated as follows:

$$MBT' = \frac{[GDGT\ Ia + GDGT\ Ib + GDGT\ Ic]}{[(GDGT\ Ia + GDGT\ Ib + GDGT\ Ic) + (GDGT\ IIa + GDGT\ IIb + GDGT\ IIIb) + (GDGT\ IIIa)]}$$

$$CBT = -LOG\frac{[GDGT\ Ib + GDGT\ IIb]}{[GDGT\ Ia + GDGT\ IIa]}$$

The relative input of aquatically produced versus soil-derived organic matter in (marine) sediments was assessed using the branched and isoprenoid tetraether (BIT) index (Hopmans et al., 2004), which is based upon the ratio of Crenarchaeol, predominantly produced by marine Thaumarchaeota and branched GDGTs (brGDGTs), which predominantly derive from the continent. BIT is calculated as:

$$BIT = \frac{[GDGT\ Ia + GDGT\ IIa + GDGT\ IIIa]}{[GDGT\ Ia + GDGT\ IIa + GDGT\ IIIa] + [Cren']}$$

Typically, BIT values <0.3 are considered to reflect marine conditions (e.g., Weijers et al., 2006; Zhu et al., 2011) while BIT values towards 0.9 to 1 indicate predominantly terrestrial input.

4. Results

4.1. δ²H of long chain n-alkanes

The apolar fractions contain a series of n-alkanes ranging from n-C_{18} to n-C_{35}, with the long-chain (C_{27}, C_{29} and C_{31}) n-alkanes having the highest peak abundances. These long-chain n-alkanes also show a strong odd-over-even carbon number predominance (Fig. 4A, D, G). At some levels the contribution of the shorter chain n-alkanes is occasionally

higher (Fig. 4D). From the analyzed samples, UV 13 (at 636 m, 2.09 Ma) contained organically-bound sulfur in the apolar fraction and it was not measured on mass-spectrometers (GC–MS nor GC-irMS). Sample UA 40 (at 357 m, 3.46 Ma), despite equal treatment, did not reveal odd-over-even carbon number predominance of the long-chain n-alkane and it was discarded from GC–MS and GC-irMS measurements. For eight samples the purified n-alkane fraction proved insufficient for GC-irMS measurements.

The $δ^2H$ values of the C_{29} and C_{31} n-alkanes co-vary. $δ^2H$ values of the C_{29} range between −141‰ and − 192‰ (Table 1 and Fig. 5A) while $δ^2H$ of C_{31} ranges between −146‰ and − 192‰. $δ^2H$ values of C_{29} show higher values compared to the C_{31} n-alkane (Table 1). $δ^2H$ values of C_{29} generally decrease throughout the Productive Series from −141‰ (UA 76, close to the bottom of the sampled section at 271.5 m, 3.57 Ma) to −169‰ at the very base of the Akchagylian (UP 08 at 522 m, 2.9 Ma; Fig. 5A). Towards the top of the section (522–715 m), covering the entire Akchagylian and the sampled part of Apsheronian, the $δ^2H$ values of of C_{29} n-alkanes stay relatively constant at −174‰ with small variations of ±6‰ (Table 1, Fig. 5A).

4.2. δ¹³C of long chain n-alkanes

The stable carbon isotopic composition of the C_{29} and C_{31} n-alkanes varies by only ±0.3‰ for both $δ^{13}C_{C29n\text{-alkanes}}$ (average of −31.3‰) and $δ^{13}C_{C31n\text{-alkanes}}$ (average of −31.8‰) (Table 1). The $δ^{13}C$ values of the
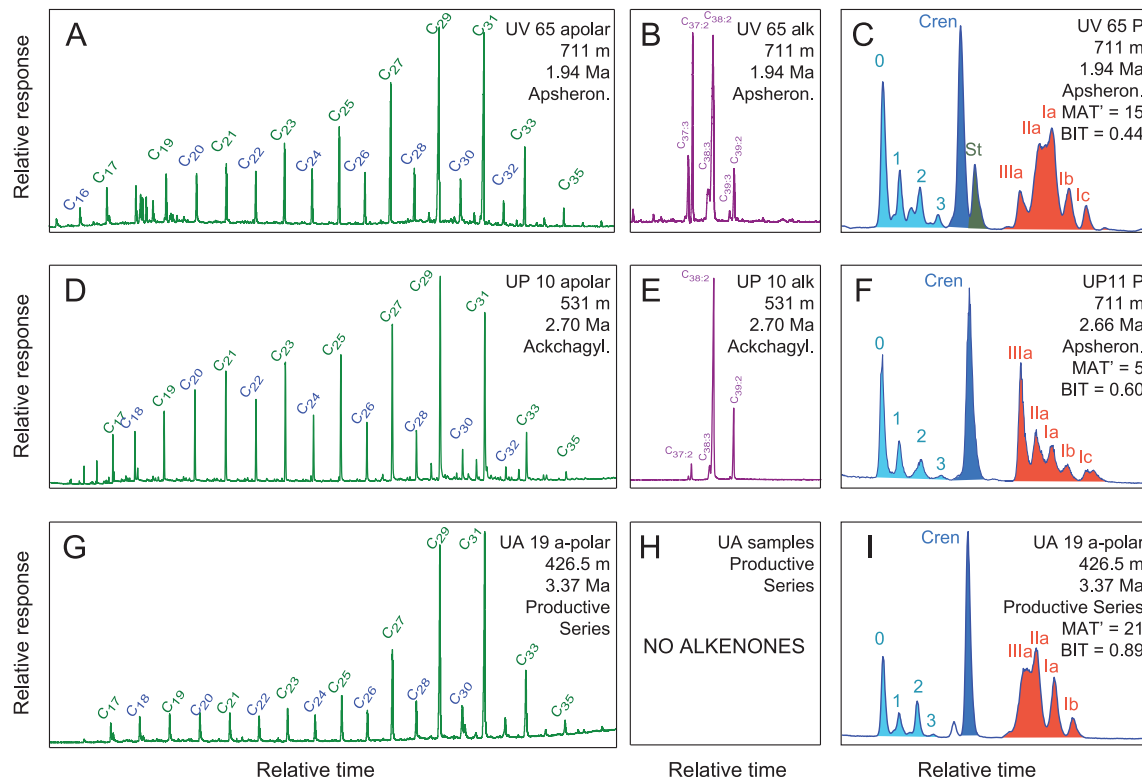

Fig. 4. Representative chromatograms of typical samples for Lokbatan section. A, D, G) The apolar fraction after second urea adduction step; note the *n*-alkanes with a distinctly odd over even predominance in chain length distribution and a higher contribution of shorter chain *n*-alkanes in some sample. B) E) and H) the alkenones fraction from the same rock sample as in panels A and D. Remark the difference between two examples in the alkenones relative contribution. C, F, I) and F) HPLC-MS base peak chromatographs of tetraether lipid of the two samples showing the dominance of isoprenoid (0,1,2,3) vs. branched (III, II, I, Ib, Ic) GDGT's membrane lipids. The Cren indicates crenarchaeol while * the standard. Note the higher contribution of isoprenoidal GDGT's in the samples.

Table 1
δ^2H and $\delta^{13}C$ isotopes measured on long chain *n*-alkanes from Lokbatan section.

Sample code	Stratigraphic level (m)	Age (Ma)	$\delta^2H_{C29n\text{-}alkane}$ (‰)	STDEV $\delta^2H_{C29n\text{-}alkane}$	N $\delta^2H_{C29n\text{-}alkane}$	δ^2H_{pp} (‰) (Sachse et al., 2006)	δ^2H_{pp} (‰) (Feakins and Sessions, 2010)	$\delta^{13}C_{C29n\text{-}alkane}$ (‰)	$\delta^2H_{C31n\text{-}alkane}$ (‰)	STDEV $\delta^2H_{C31n\text{-}alkane}$	N $\delta^2H_{C31n\text{-}alkane}$
UA 79	258	3.59	−156.3	5.6	2	−30	−69	*n.d.*	−163.8	1.8	2
UA 76	271.5	3.57	−141.5	*n.d.*	1	−13	−52	*n.d.*	−141.7	*n.d.*	1
UA 71	284	3.56	−160.5	0.6	4	−35	−73	*n.d.*	−141.7	*n.d.*	1
UA 47	332.5	3.49	−168.3	1.3	3	−44	−82	*n.d.*	−169.7	6.6	3
UA 36	373	3.44	−161.4	0.0	2	−36	−74	*n.d.*	−180.6	*n.d.*	1
UA 19	426.5	3.37	−174.1	*n.d.*	1	−51	−88	*n.d.*	−172.1	*n.d.*	1
UP 04	505.5	3.27	−162.5	2.0	3	−37	−76	*n.d.*	−171.7	4.3	3
UP 08	522	2.91	−168.7	3.9	3	−45	−82	*n.d.*	−167.1	2.8	3
UP 14	546	2.43	−174.1	3.2	3	−51	−88	*n.d.*	−173.6	1.9	3
UP 17	556.5	2.38	−174.5	2.8	3	−51	−89	*n.d.*	−177.3	2.7	3
UP 18	558.5	2.38	−191.6	3.4	3	−71	−108	*n.d.*	−191.5	3.7	3
UP 29	587	2.26	−174.8	2.3	3	−51	−89	*n.d.*	−159.6	6.7	3
UP 35	600.5	2.20	−180.4	3.2	3	−58	−95	*n.d.*	−180.4	1.4	3
UV 01	626.5	2.11	−170.5	4.6	3	−47	−84	−31.2	−175.9	5.2	2
UV 05	629.5	2.10	−176.2	6.8	4	−53	−91	*n.d.*	−181.5	5.6	4
UV 09	633	2.10	−173.7	1.3	2	−50	−88	*n.d.*	−179.6	0.5	2
UV 17	643	2.08	−166.9	3.2	3	−42	−80	−30.9	−175.3	2.7	3
UV 22	657.5	2.05	−168.8	2.8	4	−45	−83	*n.d.*	−172.6	3.2	4
UV 29	673.5	2.02	−169.4	9.4	2	−45	−83	*n.d.*	−178.9	4.4	2
UV 34	682.5	2.00	−172.5	4.5	2	−49	−87	*n.d.*	*n.d.*	*n.d.*	*n.d.*
UV 44	692.5	1.98	−174.1	4.7	2	−51	−88	−31.3	−182.3	0.8	2
UV 51	699	1.97	−174.4	4.4	4	−51	−89	*n.d.*	−177.7	6.3	4
UV 54	702	1.96	−169.0	0.0	2	−45	−83	*n.d.*	−177.8	2.9	2
UV 62	708	1.95	−168.2	5.7	2	−44	−82	−31.2	−179.2	3.8	2
UV 65	711	1.94	−170.9	3.6	3	−47	−85	*n.d.*	−179.2	0.6	3
UV 70	715	1.93	−171.6	8.5	2	−48	−86	−31.7	−175.3	3.6	2

Average of $\delta^2H_{C29n\text{-}alkane}$, $\delta^2H_{C31n\text{-}alkane}$, standard deviation (STDEV) and number of measurements (N) are listed. The δ^2H precipitation values are calculated for two scenarios 1) in the case of the European 'wet' temperate climate using the relation of Sachse et al. (2006) and 2) in the case of arid 'dry' climate using the relation of Feakins and Sessions (2010). Different scales are indicated for dry and humid climate effect on evapotranspiration. $\delta^{13}C_{C29n\text{-}alkane}$ of five levels are also listed. *n.d.* stand for not determined.

C_{29} *n*-alkanes are typically higher compared to the $\delta^{13}C$ values of C_{31} *n*-alkanes.

4.3. δ^2H on alkenones

The ketone fractions show the presence of long-chain unsaturated ethyl and methyl ketones (C_{37}-C_{39} alkenones; Fig. 4B, E). In total, only ten out of thirty-seven samples alkenones have been detected. C_{37}-C_{39} alkenones were detected from 643 m to the top of the section, covering the Apsheronian (Figs. 5, 6A). The alkenone distribution shows a remarkable dominance of the C_{37} ketone followed closely by C_{38} (Fig. 4B) with appreciable contribution of the C_{39} ketone. Both C_{37} and C_{38} ketones are dominated by the two times unsaturated components (Fig. 4B), showing relative abundances typical of marine alkenone producers. A single, solitary level, containing alkenones was identified at 531 m, 2.70 Ma, despite screening for alkenones in detail around this level. The alkenone fraction at this specific level (UP 10, at 531 m, 2.70 Ma) shows an unusual relative distribution with C_{38} being dominant (Fig. 4E), different from the alkenone distribution found in all nine samples located from 643 m, 2.08 Ma to the top of the section (Fig. 4B).

From the ten analyzed samples, nine samples from the interval 643–711 m, 2.08–1.94 Ma contained sufficient alkenones for the acquisition of δ^2H data. The $\delta^2H_{C37alkenone}$ values range between −197‰ and − 175‰ (VSMOW; Table 2 and Fig. 5B) whereas the $\delta^2H_{C38alkenone}$ values cover a larger range between −214‰ and − 177‰. Throughout the record, the δ^2H values of the C_{37} and C_{38} alkenones closely correspond, showing the same trend through time, albeit with a small offset (Table 3).

4.4. GDGT lipids

Isoprenoid and branched GDGTs are well represented over the entire sampled section (Fig. 4). We analyzed both isoprenoid and branched GDGTs within a single acquisition run for each sample (Fig. 4C, F, I).

Only for six out of the 32 analyzed samples, the calculated BIT index was lower than 0.3, therefore we refrain from calculating SSTs using TEX_{86} (Weijers et al., 2006).

4.4.1. MAT' estimates based on soil derived branched GDGT lipids

The MBT'- CBT-based MAT' estimates suggest large continental temperature variability over the sampled time interval (Table 3, Fig. 5C). Reconstructed MAT' values show overall decreasing temperatures from a maximum of 27 °C to ca. 9 °C for the Productive Series interval (from the basal sample UA79 at 258 m, 3.59 Ma until UP04 at 505.5 m, 3.27 Ma). The interval between 3.28 Ma and 2.95 Ma is missing in the section due to the erosive nature of the Akchagylian transgression and uncertain polarity patterns. In the Akchagylian that straddles the Pio-Pleistocene transition, the temperatures first decrease from 20 °C at 2.9 Ma (522 m) to 5 °C at 2.4 Ma (551 m) and afterwards values stabilize around 7 °C with a variation of ±2.5 °C. Closer to the Akchagylian – Apsheronian transition, the MAT rises again up to 12 °C (2.2 Ma, 605.5 m) and continues to increase in Apsheronian up to 17 °C (711 m, 1.94 Ma), after which the values drop again sharply to 7 °C at the top of the section (1.93 Ma, 715 m).

4.4.2. BIT estimates

The BIT values indicate large variability over the sampled interval with BIT values between 0.18 and 0.97 (Table 3, Fig. 5D). BIT values for the Productive Series interval are typically >0.85 (except UA 23 at 414.5 m, 3.39 Ma with BIT = 0.31). In the Akchagylian, the BIT values drop from 0.9 at 2.9 Ma (522 m) to 0.18 at ~2.36 Ma (565 m). Overall, the Akchagylian BIT values fluctuate around 0.42. The Apsheronian values show two distinct peaks: 0.71 at 2.11 Ma (626.5 m) and 0.96 at 2.0 Ma (682.5 m) and further decrease to 0.29 towards the top of the investigated section.

4.4.3. pH' estimates based on soil derived branched GDGT lipids

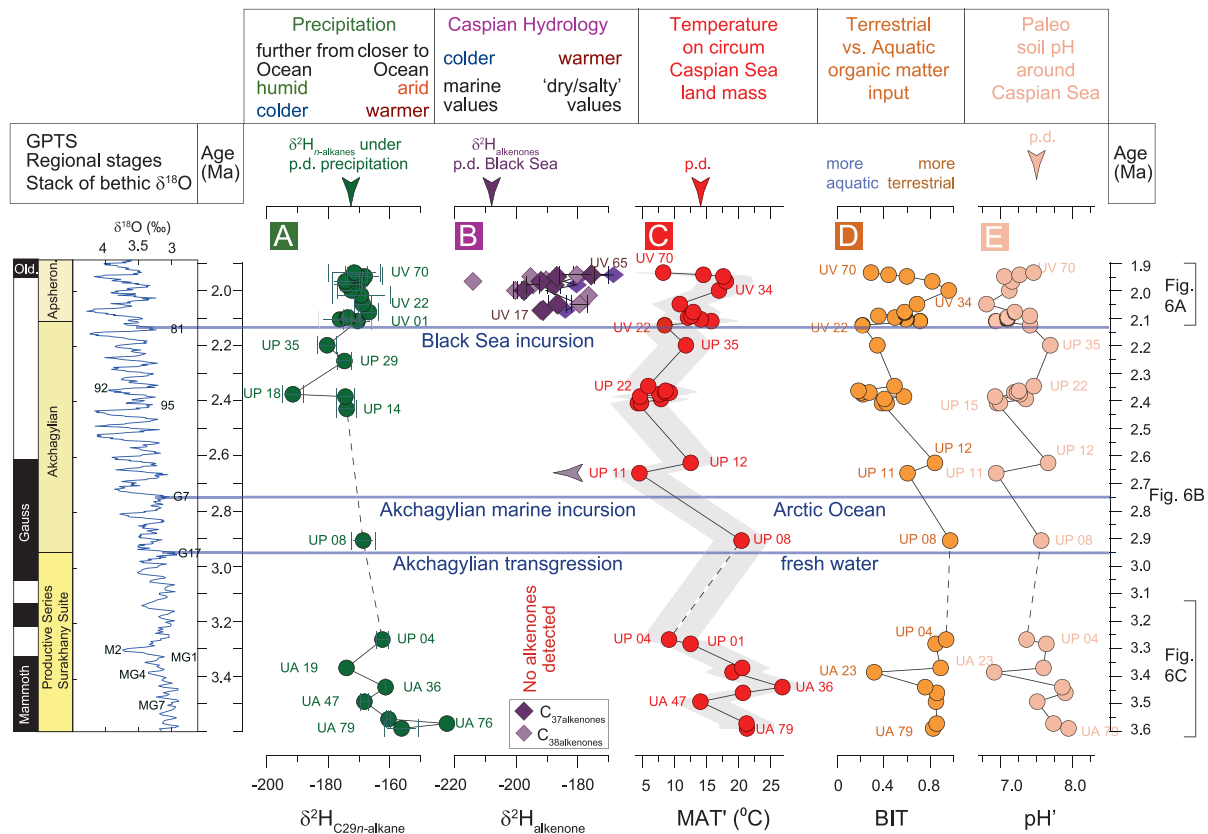The CBT-based pH' values indicate a 1.1 pH' unit variation over the

Fig. 5. Results summarizing δ²H measured on *n*-alkanes, alkenones, MAT', BIT and pH' from the Lokbatan section plotted vs. age. Geomagnetic polarity time scale (GPTS), regional stratigraphic scheme and δ¹⁸O curve of Lisiecki and Raymo (2005) are shown for correlation with the events recorded in Lokbatan. A) δ²H$_{n\text{-}C29n\text{-}}$ $_\text{alkanes}$, B) δ²H$_{C37alkenone}$ are represented and used as primary indicators for switches in hydrological balance; C) MAT' and proxy root mean square error as grey band; D) BIT index; E) paleo-soil pH' values. Given the large expected changes in the GDGT sources with the sampled 1.7 Myr interval and proxy dependent calibration coefficients, we emphasize that the relative changes of MAT' and pH' records should be primarily considered. Present-day (p.d.) values are pointed by arrow heads Remark the hiatuses in sedimentation between UP 04 (3.27 Ma) and UP 11 (2.66 Ma) without apparent unconformities when reporting to the data plotted against stratigraphic age in the Supplementary material.

sampled interval with pH values between 6.8 and 7.9. In general, pH' values decrease from the bottom to the top of the section albeit with a large variation (Table 3; Fig. 5E).

5. Discussion

5.1. δ²H and δ¹³C values of n-alkanes

In the Lokbatan section, *n*-alkanes show a general dominance of long chain *n*-alkanes with an odd over even carbon-number predominance (Fig. 4A, G) indicative for a major contribution through higher plants (Eglinton and Hamilton, 1967). However, at some levels the contribution of the shorter chain *n*-alkanes is higher (Fig. 4D) indicating that some other plant groups (i.e., aquatic) or algae contribute to the total *n*-alkane fraction.

Diverse environmental studies evaluate the role of δ²H$_{precipitation}$, climate and plant life-form in influencing δ²H values of C29 *n*-alkanes (δ²H$_{C29n\text{-}alkanes}$), the most commonly analyzed terrestrial biomarker (e. g., Sachse et al., 2012 and references there in). Globally, site-averaged δ²H$_{C29n\text{-}alkanes}$ and mean annual δ²H$_{precipitation}$ values are positively correlated, indicating that mean annual δ²H$_{precipitation}$ is the fundamental control on plant-wax δ²H values Sachse et al., 2012). However, there are differences in the slope, intercept and significance of this relationship among plant forms like trees, shrubs, forbs and graminoids (e.g., Polissar and Freeman, 2010; Feakins et al., 2019). These differences result from diverse physical and biological controls on plant source-water, leaf-water and biochemical fractionations, all being

important factors of the overall net fractionation and of plant-wax δ²H (i.e., δ²H$_{n\text{-}alkanes}$) values (Sachse et al., 2012). Importantly, a broad trend to less negative δ²H$_{n\text{-}alkanes}$ values in drier regions was observed (e.g., Feakins and Sessions, 2010; Sachse et al., 2006). Changes in temperature and source water will determine changes in the δ²H$_{precipitation}$ (Bowen, 2008), with cooler conditions leading to lows in δ²H$_{precipitation}$ (i.e., δ²H$_{C29n\text{-}alkanes}$), while increasing distance from the precipitation source would lead to δ²H$_{precipitation}$ (i.e., δ²H$_{C29n\text{-}alkanes}$) decrease.

Regardless of all above mentioned limitations, the >50‰ variation in δ²H$_{n\text{-}alkanes}$ (−142‰ at 271.5 m (3.57 Ma) to −192‰ at 558.5 m (2.38 Ma); Table 1 and Fig. 5A) from the Lokbatan section indicates important changes in the hydrology or/and the vegetation composition in the basin catchment. To estimate the δ²H$_{precipitation}$ we assume constant biosynthetic fractionation between source water and *n*-alkanes of 157‰ (Sachse et al., 2006; Sessions et al., 1999). Additionally, we evaluate two options for deuterium enrichment through evapotranspiration in our δ²H$_{precip}$ calculations (Table 1): (1) ~30‰ (Sachse et al., 2006) found under present-day Western Europe humid conditions and (2) ~60‰ as described for arid ecosystem (Feakins and Sessions, 2010). Assuming option 1 (Western Europe) reconstructed δ²H$_{precip}$ values vary between −71‰ and − 13‰. Currently, δ²H$_{precip}$ values at the closest station north of the Caspian Sea attain −62‰, while south of the Caspian Sea δ²H$_{precip}$ values are higher reaching −52‰ (IAEA, 2019; Fig. 1). Assuming option 2 (prevailing arid ecosystem) the calculated δ²H$_{precip}$ would have varied between −107‰ and − 52‰, values mostly observed in colder northern high latitudes in Eurasia (IAEA, 2019; Fig. 1).
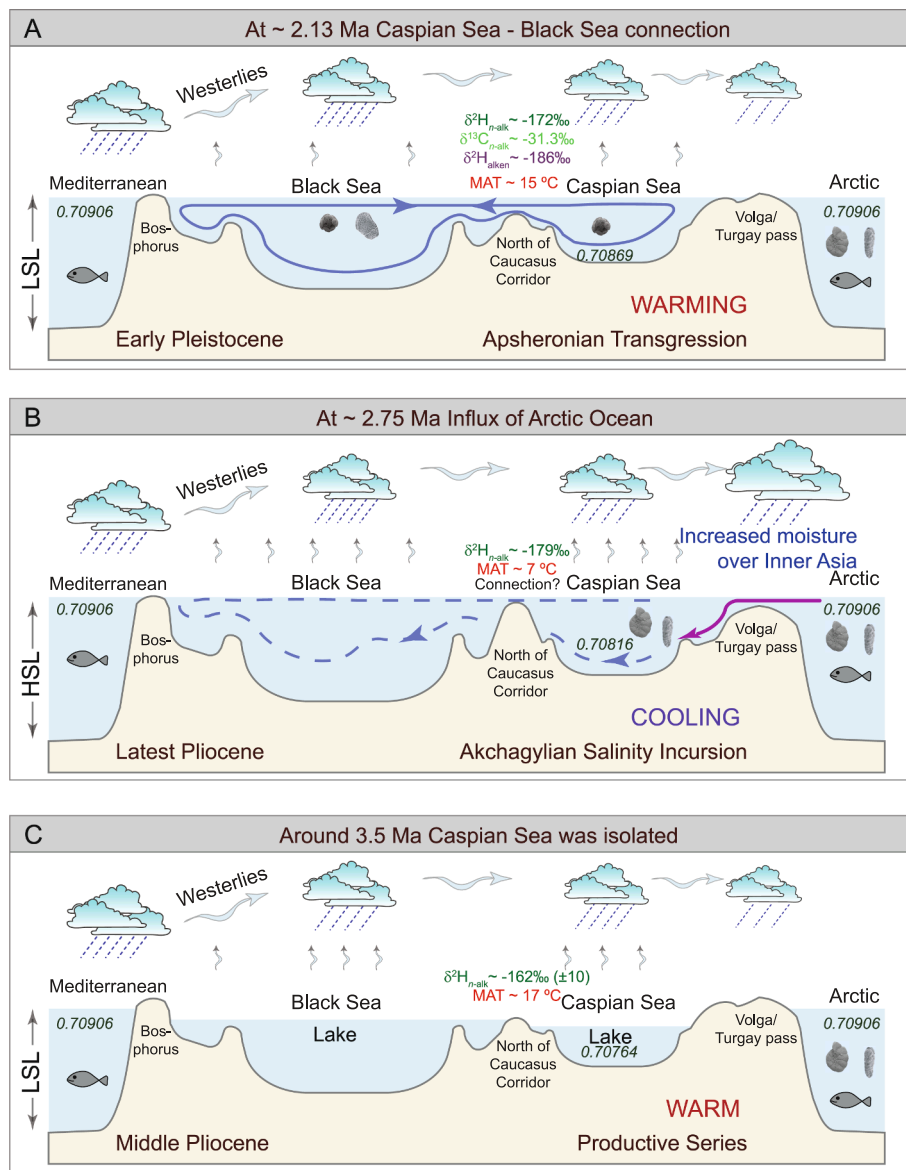
Fig. 6. Schematic scenarios at different time slices corresponding to changes in the connectivity of the Caspian Sea basin. A) At ~2.13 Ma a connection to the Black Sea was established leading to biotic exchange including import of alkenone producers (suggested by the coccoliths image) and invasion of ostracod fauna (*Tyrrhenocythere* sp., typical Black Sea fauna) into the Caspian Sea; B) At ~2.75 Ma, during the Akchagylian marine incursion the Caspian Sea received an influx of water from the Arctic Ocean facilitating the migration of biota (suggested by the foraminifera images) from the cold northern regions while a connection to the Black Sea is questioned despite evidence that Caspian Sea occupied the Azov Sea (at present in the Black Sea domain); C) At ~3.5 Ma, during the deposition of the Productive series, Caspian basin was a lake. LSL and HSL stand for low sea level and high sea level, respectively. Known $^{87}Sr/^{86}Sr$ values are represented with italic and are from Farrell et al. (1995) for the oceanic Plio-Pleistocene and van Baak et al. (2019) for the Caspian domain.

Table 2
δ^2H isotopes measured on alkenones from Lokbatan section.

Sample code	Stratigraphic level (m)	Age (Ma)	$\delta^2H_{C37alken.}$ (‰)	STDEV	N	$\delta^2H_{C38alken.}$ (‰)	STDEV	N
UV17	643	2.08	−191.3	n.d.	1	−192.1	2.2	2
UV22	657.5	2.05	−186.6	2.8	2	−179.4	8.3	2
UV29	673.5	2.02	n.d.	n.d.	n.d.	−176.5	n.d.	1
UV34	682.5	2.00	−197.4	0.7	2	−200.3	0.3	2
UV44	692.5	1.98	−187.6	2.1	2	−194.5	1.4	2
UV51	699	1.97	−192.0	n.d.	1	−214.0	n.d.	1
UV54	702	1.96	n.d.	n.d.	n.d.	−190.3	3.7	2
UV62	708	1.95	−186.8	n.d.	1	−195.3	3.6	2
UV65	711	1.94	−175.6	5.7	2	−180.3	6.4	2

Average of $\delta^2H_{C37alkenoes}$, $\delta^2H_{C38alkenones}$, standard deviation (STDEV) and number of measurements (N) are listed.

Noticeable for the Lokbatan $\delta^2H_{n-alkanes}$ record is sample UP 18 at 558.5 m, 2.38 Ma with the lowest $\delta^2H_{n-alkanes}$ (−192‰) value. Such low values are likely to be related to either high rainfall or cooler conditions in the proximity of the vapour source. This specific interval coincides with a particular diversification in the ostracod assemblage (Fig. 3).

In contrast to δ^2H, the $\delta^{13}C$ values of plant waxes primarily reflect different vegetation types. Leaf waxes from C3 plants (95% of plant species on Earth, e.g., all trees) have $\delta^{13}C$ values as low as −35‰, whereas those from C4 plants (e.g., grasses, savannah, salt marsh and desert plants) are as high as −21.7‰ (e.g., Castañeda and Schouten, 2011; Polissar et al., 2019; Feakins et al., 2020). The vegetation composition is important because the discrimination against deuterium during photosynthesis is greater in C3 plants (−117‰ to −121‰) than in C4 plants (−86‰ to −109‰) (Polissar and Freeman, 2010). The

Table 3

MAT', pH' and BIT estimates on Lokbatan section.

Sample code	Stratigraphic Level (m)	Age (Ma)	MAT' (Peterse et al., 2012)	pH' (Peterse et al., 2012)	BIT (Hopmans et al., 2004)
UA 79	258.0	3.59	21.3	7.9	0.83
UA 76	271.5	3.57	21.2	7.7	0.86
UA 47	332.5	3.49	14.1	7.5	0.85
UA 40	357.0	3.46	20.7	7.9	0.86
UA 36	373.0	3.44	26.8	7.9	0.76
UA 23	414.5	3.39	19.0	6.9	0.31
UA 19	426.5	3.37	20.5	7.6	0.89
UP 01	493.5	3.28	12.5	7.6	0.85
UP 04	505.5	3.27	9.2	7.4	0.94
UP 08	522.0	2.91	20.4	7.6	0.97
UP 11	532.5	2.66	4.6	6.9	0.60
UP 12	534.0	2.63	12.5	7.7	0.84
UP 15	551.0	2.41	4.3	7.0	0.38
UP 15_2	551.0	2.41	4.8	7.0	0.42
UP 16	554.5	2.39	7.9	7.4	0.40
UP 17	556.5	2.38	4.6	6.9	0.57
UP 18	558.2	2.38	7.7	7.3	0.22
UP 19	560.0	2.37	8.6	7.2	0.20
UP 19_2	560.0	2.37	9.3	7.2	0.27
UP 20	561.5	2.36	8.6	7.3	0.18
UP 22	565.5	2.35	5.9	7.5	0.49
UP 35	600.5	2.20	11.8	7.7	0.34
UP 42	619.0	2.13	8.5	7.4	0.21
UV 01	626.5	2.11	15.8	6.9	0.71
UV 05	629.5	2.10	14.1	7.1	0.59
UV 09	633.0	2.10	12.1	7.1	0.50
UV 13	636.0	2.09	12.6	7.4	0.35
UV 17	643.0	2.08	12.9	7.2	0.58
UV 22	657.5	2.05	10.8	6.8	0.69
UV 34	682.5	2.00	16.9	7.1	0.96
UV 51	699.0	1.97	18.0	7.2	0.82
UV 62	708.0	1.95	17.6	7.1	0.60
UV 65	711.0	1.94	14.5	7.3	0.44
UV 70	715.0	1.93	8.3	7.5	0.29

$\delta^{13}C_{n\text{-alkane}}$ values will, therefore, be controlled by the C_3 vs. C_4 plant ratio while the vegetation composition typically responds to hydrological conditions that are reflected in the $\delta^2H_{n\text{-alkane}}$ values.

In the Lokbatan section, *n*-alkanes were sufficient for additional $\delta^{13}C_{C27n\text{-alkanes}}$ only at five levels, all in the Apsheronian (626. 5 to 715 m, 2.11–1.93 Ma; Table 1). However, their values indicate unchanged, C_3-dominated vegetation for Apsheronian with mean 31.3‰ ± 0.3 for the $\delta^{13}C_{C29n\text{-alkanes}}$. The C_3 dominated vegetation situation is similar to present day, despite arid conditions prevailing in parts around the Caspian Sea.

Detailed palynological data of the Lokbatan section indicate that the regional vegetation composition responded to glacial-interglacial cycles with alternation of temperate forest assemblages (*Quercus*, *Ulmus-Zelkova*, *Alnus*, Juglandaceae) that contrast *Ephedra* and Amaranthaceae assemblages as indicators of dry environments (Hoyle et al., 2020). The persistence of mesophilous forests during glacial times indicates that glacial refugia existed in the South Caspian Basin and that the vegetation response to glaciations was muted by increased moisture availability linked to Caspian transgressions (Hoyle et al., 2020). C_3 plants dominated the overall vegetation composition indicating that vegetation change was an unlikely driver for the observed 50‰ variability in $\delta^2H_{n\text{-alkanes}}$ values.

5.2. *δ^2H values of alkenones*

Alkenones are synthesized by unicellular eukaryotic haptophyte prymnesiophyte algae, which are common in the photic zone of the modern oceans (Marlowe et al., 1984; Volkman et al., 1980). Alkenones have also been reported globally from brackish and freshwater lakes (e. g., Kristen et al., 2010). Changes in the relative abundance of alkenones

with a different degree of unsaturation are commonly used to deduce past sea surface water temperature (Brassell et al., 1986; Prahl and Wakeham, 1987).

The important observation in the Lokbatan record is that alkenones suddenly appear and prevail in the succession starting at 643 m, 2.08 Ma (Fig. 5B). The relative abundances of the C_{37}, C_{38} and C_{39} alkenones (Fig. 4B) mimic those of laboratory cultures of *Gephyrocapsa oceanica* (Sawada et al., 1996) where C_{38} alkenones dominate or are equal to the C_{37} alkenones while in general, the abundance of *G. oceanica* tends to increase progressively from the open ocean to the coast line (Sawada et al., 1996). However, both $C_{37:2}$ and $C_{38:2}$ alkenones dominate the record of Lokbatan. The relative abundance of the $C_{39:2}$ alkenone is higher than observed in open marine settings and similar to what has been found in the Black Sea (Huang et al., 2021) and in highly alkaline lakes (Thiel et al., 1997). However, whereas high alkalinity lakes show a dominant $C_{37:4}$ alkenone, this compound is absent in the Lokbatan record. The relative alkenone distribution does not correspond to present-day open marine settings but shows influence of more coastal settings where $C_{37:2}$ and $C_{38:2}$ have similar contribution.

The relative abundances of C_{37}, C_{38} and C_{39} are constant throughout the record for the entire sampled Apsheronian (Fig. 4B). Because of the unknown alkenone producer(s), we refrain from calculating temperatures based on the $U^{K'}_{37}$ index. In Lokbatan the $C_{37:2}$ is dominant, but still appreciable amounts of $C_{37:3}$ were detected, more in line with a haptophyte origin and relative medium-warm but not hot temperatures. The single level at 531 m, 2.70 Ma is at odds, showing an unusual relative distribution with a strong C_{38} dominance (Fig. 4E).

The δ^2H values of alkenones principally reflect the δ^2H of the ambient water (Englebrecht and Sachs, 2005; Paul, 2002) although δ^2H values are also influenced by the salinity, growth rate (Schouten et al., 2005) and possibly irradiance (Pagani, 2002). $\delta^2H_{alkenone}$ values may therefore be used as proxy to reconstruct δ^2H_{water} (Englebrecht and Sachs, 2005; Schouten et al., 2005; Paul, 2002; Schwab and Sachs, 2011; Weiss et al., 2019). δ^2H measured on alkenones produced in the present day oceans range from approximately −181‰ in the warm Sargasso Sea (at 31° N; Englebrecht and Sachs, 2005) to approximately −200‰ in temperate Chesapeake Bay (at 43° N; Schwab and Sachs, 2011). In the Black Sea, $\delta^2H_{alkenone}$ values today are approximately −225‰ significantly lower than the global oceans at the same latitude, most likely because of the influence of an important fresh water input (van der Meer et al., 2008).

The results from Lokbatan show that the hydrogen isotopic composition of the C_{37} alkenones ($\delta^2H_{C37alkenone}$ varies by only 21‰ (Table 1; Fig. 5B). Low $\delta^2H_{C37alkenone}$ values (−214‰) and more isotopic contrast are observed for $\delta^2H_{C38alkenone}$ (−38‰). The lowest value of −214‰ (699 m, 1.97 Ma) is identical to $\delta^2H_{C38alkenone}$ in the Black Sea over the past 3000 years (van der Meer et al., 2008) suggesting that potential early Pleistocene (Apsheronian) connectivity of the Caspian Basin to open marine settings may have been similar to the present-day Black Sea–Mediterranean Sea connection. Irrespective of the applied relationship between the δ^2H_{water} and $\delta^2H_{alkenone}$ (Englebrecht and Sachs, 2005; Schouten et al., 2005), the alkenone occurrence alone indicates a fast switch of Caspian Sea hydrology at the time of their first appearance at 643 m (2.08 Ma). The relative contribution of the alkenone and the similarity of $\delta^2H_{alkenones}$ to the Black Sea (e.g., Huang et al., 2021) hint for a Black Sea–Caspian Sea connectivity as a mechanism for the alkenone producers influx.

5.3. *The Lokbatan MAT', BIT and pH'*

Branched glycerol dialkyl glycerol tetraethers (brGDGTs) are important biomarkers to reconstruct continental paleoenvironmental conditions (e.g., Weijers et al., 2007a; Peterse et al., 2012; Inglis et al., 2017). These lipids occur widely in soils and peats (e.g., Weijers et al., 2006; Weijers et al., 2007a; Peterse et al., 2012; Naafs et al., 2017) and can be also produced in rivers and lakes (e.g., Tierney and Russell, 2009;

Liu et al., 2014; Dong et al., 2015; Weber et al., 2018). Although identifying the organisms producing brGDGTs has proven challenging, brGDGTs are likely to be membrane lipids derived from heterotrophic bacteria (Oppermann et al., 2010; Huguet et al., 2013). Certain cultured *Acidobacteria* have been found to produce the tetra-methylated brGDGT Ia (Sinninghe Damsté et al., 2011). Nevertheless, other bacterial strains synthesizing brGDGTs cannot be excluded and the exact source organisms for the brGDGTs remain to be defined.

The most important element of the Lokbatan MAT' record is the marked cooling trend over the transition between the Pliocene and Pleistocene (Fig. 5C), from ca. 21 °C (UP 08 at 522 m, 2.91 Ma) to ca. 7 °C (UP 20 at 561 m, 2.36 Ma). This cooling is accompanied by a sudden, sharp shift in the BIT index from 0.9 to 0.3, indicating a change from a clear soil to more aquatic origin of the organic matter input into the basin (Fig. 5D). Throughout the Akchagylian interval, the MAT' values increase up to ~13 °C and a change towards more aquatic contribution of the organic matter is indicated by BIT index with significantly lower values (~0.5) than the Productive Series (close to 1). The warming trend continues throughout the Apsheronian, with MAT' values increasing to 17 °C (Fig. 5C). The BIT index increases to 0.9 at level 680 m, 2.00 Ma, values typical for high contribution of continental derived organic matter indicate the proximity of the shore line. Then BIT suddenly drops to a minimum value of 0.29, which is typical for a more aquatic contribution of the organic matter.

The MAT' estimates vary around an average of ~17.3 °C (displaying a large variation of ±6) for the Productive Series and are typically higher compared to the average present-day values of 14 °C for the western coast of the Caspian Sea at the current location of Lokbatan. Conversely, MAT' estimates in the Akchagylian cluster around 7.2 °C, some 7 °C lower than present day values. During the Apsheronian MAT' values attain values very close to the present-day MAT of 14 °C. These values match the only available time-equivalent (ca. 2 Ma) pollen-based MAT in the region (Armenia; Bruch and Gabrielyan, 2002) with temperatures fluctuating around 13 °C. Bearing in mind there are large root mean square errors (RMSE) on absolute MBT'/CBT- derived MAT' reconstructions on the order of 5 °C (Peterse et al., 2012), we especially consider the relative trends in our records important. The MAT values are to be considered with caution under the assumption that large changes are expected for the ~1.7 Myr studied interval (e.g., Vasiliev et al., 2020).

Since the brGDGTs (the biomarkers used for the reconstructed MAT', BIT and pH') are dominantly generated in soils around the basin, the changes and areal extent of the Caspian Sea catchment becomes important in our interpretation. At present, the Volga River is the dominant fresh water source (82%) for the Caspian Sea and drains regions where MAT is frequently below 4 °C (Atlas of the Biosphere). However, during the Plio-Pleistocene transition, the Volga paleo-delta and the contemporaneous northern coastline lay over 1000 km north of the study location (Popov et al., 2006).

The reconstructed pH' values indicate a generally decreasing trend throughout the section. Although the pH' shows substantial variation, the calculated values indicate neutral to highly alkaline soils, typical for dry regions like the present day location of Lokbatan in Azerbaijan. The reconstructed pH' values describe essentially alkaline paleosoils as source in the ~1.7 Myr covered in the Lokbatan section. The results are similar to the present situation with the Caspian Sea surrounded by areas covered almost exclusively by alkaline soils vegetated by steppe (with precipitation less than 350 mm/year) or even occupied by semi-deserts, especially to the east of the Caspian Sea. The only exception is the Caucasus region that has mildly acidic soils, hosting the forested areas in the high altitude regions (Atlas of the Biosphere).

6. Plio-Pleistocene paleoenvironmental changes in the Caspian Basin

Sustained and coordinated efforts led to refined age models for the

Pliocene to Pleistocene regional stage boundaries in the easternmost part of the Parathethys. The resulting age model has led to a better understanding of the timing of events that affected the Caspian Basin (van Baak et al., 2013; van Baak et al., 2019; Krijgsman et al., 2019; Lazarev et al., 2019; Hoyle et al., 2020; Hoyle et al., 2021; Lazarev et al., 2021). Based on combined magnetostratigraphy, biostratigraphy and ^{40}Ar/^{39}Ar dating of multiple sections in Azerbaijan, age estimates of the regional Caspian stages have been revised: Productive Series−Akchagylian boundary is dated at 2.95 ± 0.02 Ma (Lazarev et al., 2021) and the Akchagylian−Apsheronian boundary is dated at ~2.13 Ma (Lazarev et al., 2019; Hoyle et al., 2020). In the following part we will present and discuss the paleoclimate changes identified from our biomarker research within this framework.

6.1. Dry and warm climate in the Caspian Sea region during the deposition of the Upper Productive Series (ca. 3.6 Ma to ca. 2.95 Ma)

During the deposition of the Productive Series, covering most of the Pliocene, the Caspian Sea basin was at its lowest areal extent (Figs. 2C, 6C). A lake-level lowstand was initiated around 5.3 Ma and is marked by the deposition of a sequence of interbedded and regionally continuous lacustrine mudstones and fluvio-deltaic sandstones that form the main hydrocarbon reservoirs in the South Caspian region (Aliyeva, 2005; Kroonenberg et al., 2005; Vincent et al., 2010; Jorissen et al., 2019). The deposition of the Productive Series largely overlaps with the so-called Northern Arabian Desert Climax (5.59 and 3.3 Ma), when prolonged hyperaridity characterised the Arabian Peninsula (Böhme et al., 2021). Our $\delta^2H_{C29n\text{-}alkanes}$ support the idea of significantly drier conditions during the deposition of the lower part of the Lokbatan section. Converting $\delta^2H_{C29n\text{-}alkanes}$ into $\delta^2H_{precipitation}$ using Sachse et al. (2006) provides $\delta^2H_{precipitation}$ values consistent with present-day $\delta^2H_{precipitation}$ values of dry regions (e.g., Eastern Mediterranean; Fig. 1). Furthermore, our data from the Productive Series indicate that the decreasing $\delta^2H_{C29n\text{-}alkanes}$ values (reflecting $\delta^2H_{precipitation}$) were concomitant with temperature decrease as depicted in the MAT' record (Fig. 5C). Additionally, the BIT index of the Productive Series suggests a dominantly terrestrial input of organic matter in line with a lake-level low stand and proximity to the sediment source. The soil pH estimates indicate alkaline soils (exclusively developed in dry condition) around this part of the Caspian Basin, in line with the hyperaridity recorded for the 5.59 and 3.3 Ma interval in the neighboring Arabian Peninsula (Böhme et al., 2021). Our biomarker data cannot verify the hypothesis that the Akchagylian transgression began as a freshwater event (Richards et al., 2021; Lazarev et al., 2021) due to the lack of samples from this particular interval. The only sample of the fresh water Akchagylian (UP 08 at 2. 91 Ma)shows a 20.4 °C peak in the MAT curve (Fig. 5). The sole presence of atypical alkenones at 531 m, 2.70 Ma in the Lokbatan section indicates a short influx of 'different' water source in the Caspian Sea. This level coincides with an overall low in pollen abundance followed by the largest peak in the pollen abundance (Hoyle et al., 2020). Dinoflagellates of the same samples indicate increased salinity interpreted as a marine ingression (Hoyle et al., 2020), starting at the peak of the MIS G7 interglacial (529 m), only two meters below UP 10 (at 531 m, Fig. 5), where the solitary level with the atypical relative alkenones distribution (i.e., dominance of C_{38}) appears.

6.2. Regional cooling through Arctic Ocean influx as part of the Akchagylian marine incursion

The Akchagylian transgression ended the deposition of the Productive Series and increased the areal size of the Caspian Sea five-fold (Figs. 2B, 6B) (Nevesskaya and Trubikhin, 1984; Popov et al., 2006; Green et al., 2009; Lazarev et al., 2021). Based on the presence of freshwater algae and ostracods in the post-transgressive lower Akchagylian, it seems that the Akchagylian transgression began as a freshwater event with minimal marine influence (Richards et al., 2018, 2021;

Hoyle et al., 2021). The sudden rise of the water level was explained as a result of increased atmospheric precipitation over the North Caspian catchment area linked to intensification of the Atlantic Ocean thermohaline circulation (Bartoli et al., 2005; Lazarev et al., 2021).

The following Akchagylian marine incursion was characterised by an influx of new marine biotic elements with calcareous benthic foraminifera, including species of *Cassidulina* sp. and *Cibicides* sp. and dinocysts (*Operculodinium* and *Algidasphaeridium* cf. *capillatum*), although the location and size of the connecting corridor to the open ocean are still unclear (Richards et al., 2018; Krijgsman et al., 2019;Van Baak et al., 2019).The most recent micropalaeontologic and palynologic studies conclude that these biotic assemblages were most probably derived from the Arctic Ocean, and entered the Caspian Sea via a northern seaway connection (Richards et al., 2018; Hoyle et al., 2021).

The timing of this Caspian-Arctic connection coincides with the intensification of the Northern Hemisphere Glaciations at ~2.75 Ma (Lawrence et al., 2009; De Schepper et al., 2014) and the connection was potentially established due to isostatic loading of large ice sheets (van Baak et al., 2019). Two possible options for the location of this connection have been proposed: one possible pathway is via the Volga River as Arctic Ocean water reaches the Volga catchment, which extends northwards to 60° N. The second potential pathway is east of the Ural Mountains into the Aral Sea (part of the Caspian Sea during the early Pleistocene) (Richards et al., 2021). This pathway is on the lowest water divide between the West Siberian Plain and the Aral Sea at only 50 m above global sea level (Astakhov, 2006) tracking the Turgay pass, the Paleogene gateway connecting the Arctic Ocean and the Tethys Ocean (Akhmetiev et al., 2012).

The biostratigraphic results of the Lokbatan section confirm that an important transgressive phase marks the onset of the Akchagylian (Fig. 3). The only sample (UP082.91 Ma) taken from the lowermost freshwater/low brackish water post-transgressive Akchagylian interval (520–529 m) contains no microfauna. This is in line with previous palynological and micropalaeontological data from Lokbatan and neighboring Jeirankechmez and Babazanan sections where only rare freshwater algae *Botryococcus* and the euryhaline ostracod *Cyprideis* spp. were detected. Within the so-called marine Akchagylian (529–541 m, 2.75–2.45 Ma) a completely different microfauna was documented by the sudden appearance of euryhaline foraminifera at 527 m (2.8 Ma) and 532.5 m (2.66 Ma) in the section. Importantly, these specific levels also show the sole presence of atypical, C_{38} dominated alkenones at 531 m (2.70 Ma, sample UP 10; Fig. 4E). Peak marine conditions (documented in the nearby Jeirankechmez section ~30 km southeast of Lokbatan) occurred between 2.5 and 2.6 Ma (van Baak et al., 2019). Our biomarker data support the influx of Arctic Ocean waters since the lowest MAT values in Lokbatan are concomitant with the Akchagylian marine incursion (Figs. 5C, 6B). At this level the sudden drop of the BIT index to values typical for organic matter from distal sources is in line with transgression, indicating a dominance of isoprenoidal GDGTs at the expense of the primarily terrestrially-derived, branched GDGTs.

In addition, the lowest $\delta^2H_{C29 n\text{-}alkanes}$ values in the Lokbatan record at 558.5 m (2.38 Ma) coincide with the lowest MAT' and a sharp change in BIT values towards a more dominant aquatic source of organic matter (Fig. 5). These observations indicate that after the sustained cooling trend that culminated in the Akchagylian, the Caspian basin was invaded by marine waters (i.e., marine biota occurrence). Importantly, our new data indicate that the Akchagylian water source was originating from cold regions and may have generated a massive cooling of the entire land mass around the Caspian Basin (Fig. 6B).

6.3. Water exchange with the Black Sea at the Akchagylian – Apsheronian transition

During the Apsheronian time (2.13 to 0.85 Ma) the areal extent of the Caspian Basin diminished compared to the preceding Akchagylian stage (Figs. 2A, 6A). Apsheronian deposits almost everywhere conformably overlie Akchagylian deposits (Sidnev, 1985; Alizadeh and Aliyeva, 2016). Most of the Akchagylian ostracod species continue into the Apsheronian. In the top part of the Akchagylian (616.5 m) the first common occurrences (FCO) of *Tyrrhenocythere* species are found: *Tyrrhenocythere bailovi* (Livental) and *Tyrrhenocythere azerbaijanica* (Livental) (Fig. 3). These two species become more abundant at 660 m/2.05 Ma. They develop further during the Apsheronian and are also frequent in recent sediments of the Black Sea and Caspian Sea (Gofman, 1966; van Baak et al., 2013).

Our biomarker data from Lokbatan show that the influx of alkenones with a marine-like $C_{37 alkenone}$-dominant relative contribution (at 643 m, 2.08 Ma) slightly postdates the FCO of *Tyrrhenocythere* species (at 616.5 m, 2.13 Ma; Figs. 5, 6). We propose that these Black Sea ostracod species entered the Caspian Sea together with the first alkenone producers (at 643 m, 2.08 Ma) suggesting a water exchange between the Black Sea and Caspian Sea. Questions arise on the apparent delay (26.5 m of section) of the alkenone producers. Similar delay has been previously observed in the faunal record of the Hajigabul section (Kura Basin). There, the Apsheronian begins at 2.13 Ma with oligohaline microfauna and a few indicative mollusc species of *Apscheronia* sp. and *Monodacna* sp. (Lazarev et al., 2019). Nevertheless, the major faunal influx with diverse mesohaline fauna of ostracods and foraminifera occurs slightly later, at 2.1 Ma and lasted until 2.0 Ma. Interesting similarities exist when comparing the Apsheronian connection event to the most recent reconnection of the Black Sea to the ocean via the Mediterranean Sea after the Last Glacial Maximum. A seawater connection across the shallow sill of the Bosphorus became permanently established no later than 7.150 years ago transforming the former Black Sea lake into a sea (van der Meer et al., 2008). However, the coccolithophorid *Emiliania huxleyi* invaded the Black Sea only ~2720 years ago (Jones and Gagnon, 1994). This delayed invasion has been attributed to salinity levels rising above 7.7 only later (Schulz et al., 2000), allowing *E. huxleyi* to thrive since this alkenone producer has not been reported to occur at salinities below such values (Bukry, 1974). A similar situation can be envisaged for the Black Sea – Caspian Sea connection that brought the *Tyrrhenocythere* genus into the Caspian Sea. Only when salinity levels of the of the Caspian domain rose to a certain value could alkenone producers radiate and flourish. Support for this hypothesis is provided by the δ^2H record: the average Pleistocene δ^2H_{water} of the Caspian Sea recorded at Lokbatan (−190‰) is similar to the δ^2H of the Black Sea ~2720 years ago (−202‰) appropriate salinity was attained through a functional connection to the Mediterranean ultimately allowing alkenone-producing algae to thrive. The exact alkenone producer in the Caspian Sea observed at ~2.13 Ma is not known. The closest similarity is once again the Black Sea during the transition between the last glacial maximum to Holocene when re-connection to the Mediterranean Sea occurred. Huang et al. (2021) demonstrated that, in the Black Sea, when surface water salinity declined significantly, Group II Isochrysidales become the dominant alkenone producer while during the more saline phases *E. huxleyi* was the main producer.

Alkenones, their relative distribution and their hydrogen isotope ratios provide further support that Black Sea waters reached the Caspian Sea at ~2.13 Ma. Alkenones appear after a ten-meter-thick anoxic layer (605–615 m) that marks a sharp change in water column oxygenation, most probably provoked by contrasting characteristics of the water mass (i.e., temperature and salinity) that reached the Caspian Sea. This influx also introduced the coccolithophorids which are the specific algae producing alkenones. It is noteworthy that in the present day Caspian Sea no alkenones are mentioned while such biomarkers are ubiquitous in the slightly higher saline Black Sea. The data presented here is also the first documentation of these components in the sedimentary succession of the Caspian Sea adding to the earlier identification of these components in the Black Sea (Vasiliev et al., 2013, 2015, 2019), both parts of the older Parathethys Sea. Furthermore, on the basis of the alkenone presence in the sedimentary rocks of Lokbatan and the ostracod assemblages we could further convey that the Caspian Sea was connected with the Black

Sea and potentially even to the Mediterranean at ~2.13 Ma.

6.4. The Caspian Sea as a transient long-term moisture source for Central Asia

At present, the Caspian Sea is an important source of moisture for the continental interior of inner Asia and westerlies precipitation transport has been an important element in central Asian hydroclimate over large parts of the Cenozoic (Caves et al., 2015). In Oligocene to Miocene times, however, the Caspian Basin was part of the much larger Paratethys, an epicontinental sea that controlled the sedimentation in the region, and modulated the climate and moist availability of the inner part of Eurasia for tens of millions of years (Ramstein et al., 1997). Paratethys retreat is considered to have determined rearrangements of the climate zones. The African summer monsoon was drastically weakened by the Mediterranean-Paratethys shrinkage during the Tortonian (11.61–7.25 Ma), allowing arid, desert conditions to expand across North Africa (Zhang et al., 2014). Not only did the Mediterranean-Paratethys shrinkage alter the mean climate of the region, it also enhanced the sensitivity of the African monsoon to orbital forcing, which subsequently became the major driver of the extent of the Sahara Desert (Zhang et al., 2014). Climate simulations for the early Pliocene (5–4 Ma) indicate dryer-than-present midlatitudes in the northern hemisphere (Burls and Fedorov, 2017) whereas models of the late Pliocene (3 Ma) reveal increased humidity in northern midlatitudes (Colleoni et al., 2015). However, no specific paleoclimate simulation exists to grasp the role of the Paratethys (i.e., Pontocaspian domain) for the Pliocene to Pleistocene transition, the crucial time interval when the Caspian Basin recorded its last major transgression, just before the intensification of Northern Hemisphere glaciation. After ~2.95 Ma, the Paratethys reached its maximum extent in the east (Fig. 2B), regaining the area of the present-day Aral Lake and its drainage basin and further occupying large parts of the northern Russia (Popov et al., 2010). The subsequent decrease in basin extent and the resulting decrease in potential evaporative moisture flux to the atmosphere coincide with a series of climate change events in Central Asia:

1) Between 2.75 and 2.45 Ma, the maximum areal extent of the Caspian Basin was similar to that during the Miocene (Zhang et al., 2014), the time when the intertropical convergence zone migrated northwards by more than 20^0 in latitude over the Arabian Peninsula, inducing an increase in moisture availability. After the maximum extent at ~2.7–2.6 Ma, the Paratethys retreated within the enclosed Caspian Sea, lower Volga and Black Sea boundaries (Fig. 2A). This retreat resulted in major rearrangements of regional moisture transport paths. Growing evidence indicate that westerly circulation affected moisture conditions in central East Asia, yet with variable intensity (Lu et al., 2019). Water vapour recycling and supply through westerly sources would have been reduced with the shrinkage of Caspian Sea after the Akchagylian transgression.

2) An abrupt intensification of aridification in the late Pliocene after ~2.6 Ma (Lu and Guo, 2014) may have been triggered or enhanced by the termination of the highstand conditions during the Akchagylian in the Caspian Sea. Mammal assemblages from central east Asia indicate an adaptation to cold and dry conditions during the late Pliocene already, while a dry-steppe environment developed from the early Pleistocene.

3) The accumulation of loess deposits in the northeastern Iranian Golestan Province at ~2.4 Ma suggests that an arid environment had formed in the dust source regions, such as the Karakum Desert and the Caspian Lowland, during the early Pleistocene. This remarkable early Pleistocene aridification in western Arid Central Asia is broadly consistent with the onset of aridification in Arid Central Asia (Dodonov, 1991) such as the expansion of the Taklimakan Desert in northwestern China (Sun et al., 2011).

Shrinkage of the Caspian Basin may have influenced the vapour availability carried by westerlies towards western and central Asia and led to the loss of its thermal regulator role. Yet, determining the importance of the regional sea retreat during the Pleistocene needs equivalent proxy records to quantify and qualify the changes in temperature and the impact on moisture availability around the Caspian Sea Basin.

7. Conclusions

The Plio-Pleistocene biomarker based proxies data from the Caspian Basin presented here provide independent arguments for a sequence of important rearrangements in Eurasian hydrology around the Pleistocene-Pliocene boundary:

1) The large variation (~55‰) recorded in the δ^2H of terrestrial plant wax long chain *n*-alkanes indicates significant continental hydrological changes, in the Caspian Basin catchment over the 1.7 Myr sampled interval.

2) Decreasing $\delta^2H_{C29n\text{-}alkanes}$ values (corresponding to $\delta^2H_{precipitation}$) during the deposition of the Productive Series (~5–3.2 Ma) were provoked by the concomitant temperature decrease as depicted in our MAT' record. It is a time interval of pronounced aridity in the neighboring Arabian Peninsula and, considering the trajectory of the present day precipitation transport, the reduced areal extent of Caspian Basin at that time could have been a crucial factor in causing reduced moisture availability in the region.

3) Age-equivalent MAT' and BIT data show that, at ~2.75 Ma, during the so-called Akchagylian salinity incursion, an influx of marine biota into the Caspian Basin originated from a cold region of the open ocean, in line with flooding from the Arctic ocean that generated a massive cooling of the entire land mass around it.

4) A change towards constant $\delta^2H_{n\text{-}alkane}$ (i.e., $\delta^2H_{precipitation}$) and $\delta^{13}C_{n\text{-}alkane}$ (typical for the current dominant C_3 plant contribution) correlates with the appearance of *Tyrrhenocythere* ostracods (Black Sea fauna) in the Caspian Basin. The calculated $\delta^2H_{precipitation}$ suggest a strongly similar precipitation source as in the present day Caspian Sea region from the connectivity event at 2.13 Ma.

5) The invasion of Black Sea fauna at 2.13 Ma is shortly followed by the occurrence of alkenones in the Caspian Basin at ~2.1 Ma. The relative distribution of alkenones and their δ^2H combined with changes in ostracod assemblages form a strong support for a connection of the Caspian Basin with a saline basin, most likely the Black Sea, established at~2.13 Ma, at the onset of the Apsheronian stage.

Declaration of Competing Interest

The authors declare that they have no known competing conflict of interest or personal relationship that could have appeared to influence the work reported here.

Appendix A. Supplementary data

Supplementary data to this article can be found online at https://doi.org/10.1016/j.palaeo.2021.110802.

References

Akhmetiev, M.A., Zaporozhets, N.I., Benyamovskiy, V.N., Aleksandrova, G.N., Iakovleva, A.I., Oreshkina, T.V., 2012. The Paleogene history of the Western Siberian Seaway- a connection of the Peri-Tethys to the Arctic Ocean. Aust. J. Earth Sci. 105, 50–67.

Aliyeva, E.G.M., 2005. Reservoirs of the lower Pliocene productive series at the western flank of the South Caspian basin. Lithol. Miner. Resour. 40, 267–278.

Alizadeh, A.A., Aliyeva, E.G., 2016. The evolution of benthic fauna and bionomic conditions of the South Caspian Basin in the Pliocene. In: Stratigraphy and Sedimentology of Oil-Gas Basins (Baku, Azerbaijan), 1, pp. 1–22.

Astakhov, V.I., 2006. Evidence of late Pleistocene ice-dammed lakes in West Siberia. Boreas 35, 607–621.

Bartoli, G., Sarnthein, M., Weinelt, M., Erlenkeuser, H., Garbe-Schönberg, D., Lea, D.W., 2005. Final closure of Panama and the onset of northern hemisphere glaciation. Earth Planet. Sci. Lett. 237, 33–44.

Böhme, M., Spassov, N., Majidifard, M.R., Gärtner, A., Kirscher, Marks M., Dietzel, C.U., Uhlig, G., El Atfy, H., Begun, D.R., Winklhofer, M., 2021. Neogene hyperaridity in Arabia drove the directions of mammalian dispersal between Africa and Eurasia. Nat. Comm. Earth Environ. 2, 85. https://doi.org/10.1038/s43247-021-00158-y.

Bowen, G.J., 2008. Spatial analysis of the intra-annual variation of precipitation isotope ratios and its climatological corollaries. J. Geophys. Res.-Atmos. 113, D05113. https://doi.org/10.1029/2007JD009295.

Brassell, S.C., Eglinton, G., Marlowe, I.T., Pflaumann, U., Sarnthein, M., 1986. Molecular stratigraphy e a new tool for climatic assessment. Nature 320, 129–133.

Bruch, A., Gabrielyan, I.G., 2002. Quantitative data of the Neogene climatic development in Armenia and Nakhichevan. Acta Univ. Carol. Geol. 46, 41–48.

Bukry, D., 1974. Coccoliths as paleosalinity indicators -evidence from the Black Sea. In: Memoirs of the American Association of Petroleum Geologists, 20, pp. 353–363.

Burls, N.J., Fedorov, A.V., 2017. Wetter subtropics in a warmer world: contrasting past and future hydrological cycles. Proc. Natl. Acad. Sci. 114, 12888–12893.

Castañeda, I.S., Schouten, S., 2011. A review of molecular organic proxies for examining modern and ancient lacustrine environments. Quat. Sci. Rev. 30, 2851–2891.

Caves, J.K., Winnick, M.J., Graham, S.A., Sjostrom, D.J., Mulch, A., Chamberlain, C.P., 2015. Role of Westerlies in Central Asia climate over the Cenozoic. Earth Planet. Sci. Lett. 428, 33–43.

Clauer, N., Chaudhuri, S., Toulkeridis, T., Blanc, G., 2000. Fluctuations of Caspian sea level: beyond climatic variations? Geology 28, 1015–1018.

Colleoni, F., Cherchi, A., Masina, S., Brierley, C.M., 2015. Impact of global SST gradients on the Mediterranean runoff changes across the Plio-Pleistocene transition. Paleoceanography 30, 751–767.

De Jonge, C., Hopmans, E.C., Zell, C.I., Kim, J.-H., Schouten, S., Sinninghe Damsté, J.S., 2014. Occurrence and abundance of 6-methyl branched glycerol dialkyl glycerol tetraethers in soils: Implications for palaeoclimate reconstruction. Geochim. Cosmochim. Acta 141, 97–112.

De Schepper, S., Gibbart, P.L., Salzmann, U., Ehlers, J., 2014. A global synthesis of the marine and terrestrial evidence for glaciation during the Pliocene Epoch. Earth Sci. Rev. 135, 83–102.

Dodonov, A., 1991. Loess of Central Asia. Geol. J. 24, 185–194.

Dong, L., Li, Q.Y., Li, L., Zhang, C.L., 2015. Glacial-interglacial contrast in MBT/CBT proxies in the South China Sea: Implications for marine production of branched GDGTs and continental teleconnection. Org. Geochem. 79, 74–82.

Dong, W., Lin, Y., Wright, J.S., Xie, Y., Ming, Y., Zhang, H., Chen, R., Chen, Y., Xu, F., Lin, N., Yu, C., Zhang, B., Jin, S., Yang, K., Li, Z., Guo, J., Wang, L., Lin, G., 2018. Regional disparities in warm season rainfall changes over arid eastern–Central Asia. Sci. Rep. 8, 13051.

Eglinton, G., Hamilton, R.J., 1967. Leaf Epicular Waxes. Science 156, 1322–1335.

Englebrecht, A.C., Sachs, J.P., 2005. Determination of sediment provenance at drift sites using hydrogen isotopes and unsaturation ratios in alkenones. Geochim. Cosmichim. Acta 69 (17), 4253–4265.

Farrell, J.W., Clemens, S.C., Gromet, L.P., 1995. Improved chronostratigraphic reference curve of late Neogene seawater 87Sr/86Sr. Geology 23, 403–406. https://doi.org/10.1130/0091-7613(1995)023<0403.

Feakins, S.J., Sessions, A.L., 2010. Controls on the D/H ratios of plant leaf waxes in an arid ecosystem. Geochim. Cosmichim. Acta 74, 2128–2141.

Feakins, S.J., Wu, M.S., Ponton, C., Tierney, Jessica E., 2019. Biomarkers reveal abrupt switches in hydroclimate during the last glacial in southern California. Earth Planet. Sci. Lett. 515, 164–172.

Feakins, S.J., Liddy, H.M., Tauxe, L., Galy, V., Feng, X., Tierney, J.E., Miao, Y., Warny, S., 2020. Miocene C4 grassland expansion as recorded by the Indus Fan. Paleoceanogr. Paleoclim. 35 https://doi.org/10.1029/2020PA003856 e2020PA003856.

Forte, A.M., Sumner, D.Y., Cowgill, E., Stoica, M., Murtuzayev, I., Kangarli, T., Elashvili, M., Godoladze, T., Javakhishvili, Z., 2015. Late Miocene to Pliocene stratigraphy of the Kura Basin, a subbasin of the South Caspian Basin: implications for the diachroneity of stage boundaries. Basin Res. 27, 247–271.

Gofman, E., 1966. Ecology of Modern and Novocaspian Ostracods of the Caspian Sea (in Russian). Akademie NAUK SSSR, Moscow (183 pages).

Green, T., Abdullayev, N.R., Hossack, J., Riley, G., Roberts, A.M., 2009. Sedimentation and subsidence in the South Caspian Basin, Azerbaijan. Geol. Soc. Lond., Spec. Publ. 312, 241–260.

Hinds, D.J., Aliyeva, E., Allen, M.B., Davies, C.E., Kroonenberg, S.B., Simmons, M.D., Vincent, S.J., 2004. Sedimentation in a discharge dominated fluvial/lacustrine system: the Neogene Productive Series of the South Caspian Basin, Azerbaijan. Mar. Pet. Geol. 21, 613–638.

Hopmans, E.C., Weijers, J.W.H., Schefuß, E., Herfort, L., Sinninghe Damsté, J.S., Schouten, S., 2004. A novel proxy for terrestrial organic matter in sediments based on branched and isoprenoid tetraether lipids. Earth Planet. Sci. Lett. 224, 107–116. https://doi.org/10.1016/j.epsl.2004.05.012.

Hoyle, T.M., Leroy, S.A.G., Lopez-Merino, L., van Baak, C., Cortizas, A.M., Richards, K., Aghayeva, V., 2021. Biological turnovers in response to marine incursion into the Caspian Sea at the Plio-Pleistocene transition. Glob. Planet. Change 206, 103623.

Hoyle, T.M., Leroy, S.A.G., López-Merino, L., Miggins, D.P., Koppers, A.A.P., 2020. Vegetation succession and climate change across the Plio-Pleistocene transition in eastern Azerbaijan, Central Eurasia (2.77–2.45 Ma). Palaeogeogr. Palaeoclimatol. Palaeoecol. 538, 109386.

Huang, Y., Zheng, Y., Heng, P., Giosan, L., Coolen, M.J.L., 2021. Black Sea paleosalinity evolution since the last deglaciation reconstructed from alkenone-inferred Isochrysidales diversity. Earth Planet. Sci. Lett. 564, 116881.

Huguet, A., Gocke, M., Derenne, S., Fosse, C., Wiesenberg, G.L.B., 2013. Root associated branched tetraether source microorganisms may reduce estimated paleotemperatures in subsoil. Chem. Geol. 356, 1–10.

IAEA/WMO, 2019. Global Network of Isotopes in Precipitation. The GNIP Database. Accessible at. http://www.iaea.org/water.

Inglis, G.N., Collinson, M.E., Riegel, W., Wilde, V., Farnsworth, A., Lunt, D.J., Valdes, P., Robson, B.E., Scott, A.C., Lenz, O.K., Naafs, B.A., Pancost, R.D., 2017. Mid-latitude continental temperatures through the early Eocene in western Europe, Earth Planet. Sci. Lett. 460, 86–96.

Jones, G., Gagnon, A.R., 1994. Radiocarbon chronology of Black Sea sediments. In: Deep Sea Research Part I Oceanographic Research Papers, 41, pp. 531–557. https://doi.org/10.1016/0967-0637(94)90094-9.

Jorissen, E., Abels, H., Wesselingh, F., Lazarev, S., Aghayeva, V., Krijgsman, W., 2019. Amplitude, frequency and drivers of Caspian Sea lake-level variations during the early Pleistocene and their impact on a protected wave-dominated coastline. Sedimentology. https://doi.org/10.1111/sed.12658.

Krijgsman, W., Tesakov, A., Yanina, T., Lazarev, S., Danukalova, G., van Baak, C.G.C., Agustí, J., Alçiçek, M.C., Aliyeva, E., Bista, D., Bruch, A., Büyükmeriç, Y., Bukhsianidze, M., Flecker, R., Frolov, P., Hoyle, T.M., Jorissen, E., Kirscher, U., Koriche, S.A., Kroonenberg, S.B., Lordkipanidze, D., Oms, O., Rausch, L., Singarayer, J., Stoica, M., van de Velde, S., Titov, V.V., Wesselingh, F.P., 2019. Quaternary time scales for the Pontocaspian domain: interbasinal connectivity and faunal evolution. Earth Sci. Rev. 188, 1–40. https://doi.org/10.1016/j.earscirev.2018.10.013.

Kristen, I., Wilkes, H., Vieth, A., Zink, K.G., Plessen, B., Thorpe, J., Partridge, T.C., Oberhansli, H., 2010. Biomarker and stable carbon isotope analyses of sedimentary organic matter from Lake Tswaing: evidence for deglacial wetness and early Holocene drought from South Africa. J. Paleolimnol. 44, 143–160.

Kroonenberg, S.B., Alekseevski, N.I., Aliyeva, E.G.M., Allen, M.B., Aybulatov, D.N., Baba-Zadeh, A., Badyukova, E.N., Davies, C.E., Hinds, D.J., Hoogendoorn, R.M., Huseynov, D., Ibrahimov, B., Mamedov, P., Overeem, I., Rusakov, G.V., Suleymanov, S., Svitoch, A.A., Vincent, S.J., 2005. Two Deltas, Two Basins, One River, One Sea: The Modern Volga delta as an Analogue of the Neogene Productive Series, South Caspian Basin. In: Giosan, L., Bhattacharya, J.P. (Eds.), River Deltas-Concepts, Models and Examples, p. 231e255.

Lawrence, K.T., Herbert, T.D., Brown, C.M., Raymo, M.E., Haywood, A.M., 2009. High-amplitude variations in North Atlantic Sea surface temperature during the early Pliocene warm period. Paleoceanography 24.

Lazarev, S., Jorissen, E.L., van de Velde, S., Rausch, L., Stoica, M., Wesselingh, F.P., van Baak, C.G., Yanina, T.A., Aliyeva, E., Krijgsman, W., 2019. Magneto-biostratigraphic age constraints on the palaeoenvironmental evolution of the South Caspian basin during the Early-Middle Pleistocene (Kura basin, Azerbaijan). Quat. Sci. Rev. 222, 105895.

Lazarev, S., Kuiper, K.F., Oms, O., Bukhsianidze, M., Vasilyan, D., Jorissen, E.L., Bowmeester, M.J., Aghayeva, V., van Amerongen, A.J., Agustí, J., Lordkipanitze, D., Krijgsman, W., 2021. Five-fold expansion of the Caspian Sea in the late Pliocene: New and revised magnetostratigraphic and ^{40}Ar/^{39}Ar age constraints on the Akchagylian Stage. Glob. Planet. Change 206, 103624.

Lisiecki, L.E., Raymo, M.E., 2005. A Pliocene–Pleistocene stack of 57 globally distributed benthic δ^{18}O records. Paleoceanography 20, PA1003.

Liu, X.L., Zhu, C., Wakeham, S.G., Hinrichs, K.U., 2014. *In situ* production of branched glycerol dialkyl glycerol tetraethers in anoxic marine water columns. Mar. Chem. 166, 1–8.

Lu, H.Y., Guo, Z.T., 2014. Evolution of the monsoon and dry climate in East Asia during late Cenozoic: a review. Sci. China Earth Sci. 57, 70–79. https://doi.org/10.1007/s11430-013-4790-3.

Lu, Huayu, Wang, Xianyan, Wang, Xiaoyong, Chang, Xi, et al., 2019. Formation and Evolution of Gobi Desert in Central and Eastern Asia, vol. 194, pp. 251–263. https://doi.org/10.1016/j.earscirev.2019.04.014.

Marlowe, I.T., Green, J.C., Neal, A.C., Brassel, S., Elington, G., Course, P.A., 1984. Long-chain (n-C$_{37-39}$) alkenones in the Prymnesiophyceae. Distribution of alkenones and other lipids and their taxonomic significance. Br. Phycol. J. 19, 203–216. https://doi.org/10.1080/00071618400650221.

Miller, D.R., Habicht, M.H., Keisling, B.A., Castañeda, I.S., Bradley, R.S., 2018. A 900-year New England temperature reconstruction from in situseasonally produced branched glycerol dialkyl glyceroltetraethers (brGDGTs). Clim. Past 14, 1653–1667.

Naafs, B.D.A., Inglis, G.N., Zheng, Y., Amesbury, M.J., Biester, H., Bindler, R., et al., 2017. Introducing global peat-specific temperature and pH calibrations based on brGDGT bacterial lipids. Geochim. Cosmochim. Acta 208, 285–301.

Nevesskaya, L.A., Trubikhin, V.M., 1984. History of the Caspian basin and its mollusc fauna in the late Pliocene – Early Pleistocene. In: Kamaletdinov, M.A., Yakhimovich, V.L. (Eds.), Antropogen of Eurasia. Nauka, Moscow, pp. 19–27.

Niedermeyer, E.M., Forrest, M., Beckmann, B., Sessions, A.L., Mulch, A., Schefuß, E., 2016. The stable hydrogen isotopic composition of sedimentary plant waxes as

quantitative proxy for rainfall in the West African Sahel. Geochim. Cosmochim. Acta AEM 184, 55–70.

Oppermann, B.I., Michaelis, W., Blumenberg, M., Frerichs, J., Schulz, H.M., Schippers, A., Beaubien, S.E., Kruger, M., 2010. Soil microbial community changes as a result of long-term exposure to a natural CO_2 vent. Geochim. Cosmochim. Acta 74, 2697–2716.

Pagani, M., 2002. The alkenone–CO_2 proxy and ancient atmospheric carbon dioxide. Phil. Trans. R. Soc. Lond. A. 360, 609–632.

Panin, N., 2005. The Black Sea coastal zone - an overview. Geo-Eco-Mar. 11, 21–40.

Paul, H.A., 2002. Application of Novel Stable Isotope Methods to Reconstruct Peleoenvironments: Compound-Specific Hydrogen Isotopes and Pore-Water Oxygen Isotopes. Ph. D. Thesis. Swiss Federal Institute of Technology, Zurich (141 pp).

Peterse, F., van der Meer, J., Schouten, S., Weijers, J.W.H., Fierer, N., Jacckson, R.B., Kim, J.-H., Sinninghe Damsté, J.S., 2012. Revised calibration of the MBT-CBT paleotemperature proxy based on branched tetraether membrane lipids in surface soils. Geochim. Cosmochim. Acta 96, 215–229.

Polissar, P.J., Freeman, K.H., 2010. Effects of aridity and vegetation on plant-wax dD in modern lake sedimets. Geochim. Cosmochim. Acta 74, 5785–5797.

Polissar, P.J., Rose, C., Uno, K.T., Phelps, S.R., de Medocal, P., 2019. Synchronous rise of African C4 ecosystems 10 million years ago in the absence of aridification. Nat. Geosci. 12, 657–660.

Popov, S.V., Shcherba, I.G., Iluina, L.B., Nevesskaya, L.A., Paramonova, N.P., Khondkarian, S.O., Magyar, I., 2006. Late Miocene paleogeography of the Paratethys and its relation to the Mediterranean. Palaeogeogr. Palaeoclimatol. Palaeoecol. 238, 91–106.

Popov, S.V., Antipov, M.P., Zastrozhnov, A.S., Kurina, E.E., Pinchuk, T.N., 2010. Sealevel fluctuations on the northern shelf of the eastern Parathethys in the Oligocene-Neogene. Stratigr. Geol. Correl. 18 (2), 200e224. https://doi.org/10.1134/S0869593810020073.

Prahl, F.G., Wakeham, S.G., 1987. Calibration of unsaturation patterns in long-chain ketone compositions for paleotemperature assessment. Nature 330, 367–369.

Ramstein, G., Fluteau, F., Besse, J., Joussaume, S., 1997. Effect of orogeny, plate motion and land-sea distribution on Eurasian climate change over the past 30 million years. Nature 386, 788–795.

Richards, K., Van Baak, C.G.C., Athersuch, J., Hoyle, T.M., Stoica, M., Austin, W.E.N., Cage, A.G., Wonders, A.A.H., Marret, F., Pinnington, C.A., 2018. Palynology and micropalaeontology of the Pliocene - Pleistocene transition in outcrop from the western Caspian Sea, Azerbaijan: potential links with the Mediterranean, Black Sea and the Arctic Ocean? Palaeogeogr. Palaeoclimatol. Palaeoecol. 511, 119–143.

Richards, K., Vincent, S., Davies, C., Hinds, D., Aliyeva, E., 2021. Palynology and sedimentology of the Pliocene Productive Series from eastern Azerbaijan. Palynology. https://doi.org/10.1080/01916122.2021.1884139.

Sachse, D., Radke, J., Gleixner, G., 2004. Hydrogen isotope ratio of recent lacustrine sedimentary n-alkanes record modern climate variability. Geochim. Cosmochim. Acta 68, 4877–4889.

Sachse, D., Radke, J., Gleixner, G., 2006. dD values of individual n-alkanes from terrestrial plants along a climatic gradient - implications for the sedimentary biomarker record. Org. Geochem. 37, 469–483.

Sachse, D., Billault, I., Bowen, G.J., Chikaraishi, Y., Dawson, T.E., Feakins, S.J., et al., 2012. Molecular paleohydrology: Interpreting the hydrogen-isotopic composition of lipid biomarkers from photosynthesizing organisms. Annu. Rev. Earth Planet. Sci. 40, 221–249. https://doi.org/10.1146/annurev-earth-042711-105535.

Sawada, K., Handa, N., Shiraiwa, Y., Danbara, A., Montani, S., 1996. Long-chain alkenones and alkyl alkenoates in the coastal and pelagic sediments of the northwest North Pacific, with special reference to the reconstruction of *Emiliania huxleyi* and *Gephyrocapsa oceanica*. Org. Geochem. 24, 751–764.

Schefuss, E., Schouten, S., Schneider, R.R., 2005. Climatic controls on central African hydrology during the past 20,000 years. Nature 437, 1003–1006.

Schouten, S., Ossebaar, J., Schreiber, K., Kienhuis, M.V.M., Langer, G., Bijma, J., 2005. The effect of temperature and salinity on the stable hydrogen isotopic composition of long chain alkenones produced by *Emiliania huxleyi* and *Gephyrocapsa oceanica*. Biogeosci. 2, 1681–1695.

Schulz, H.M., Schöner, A., Emeis, K.C., 2000. Long-chain alkenone patterns in the Baltic Sea - an ocean-freshwater transition. Geochim. Cosmichim. Acta 64, 469–477.

Schwab, V., Sachs, J.P., 2011. Hydrogen isotopes in individual alkenones from the Chesapeake Bay estuary. Geochim. Cosmichim. Acta 75, 7552–7565.

Sessions, A.L., Burgoyne, T.W., Schimmelmann, A., Hayes, J.M., 1999. Fractionation of hydrogen isotopes in lipid biosynthesis. Org. Geochem. 30, 1193–1200.

Sidnev, A.V., 1985. The History of the Pliocene Hydrographic System in Pre-Urals. Nauka, Moscow.

Sinninghe Damsté, J.S., Rijpstra, W.I.C., Hopmans, E.C., Weijers, J.W.H., Foesel, B.U., Overmann, J., Dedysh, S.N., 2011. 13,16-Dimethyl octacosanedioic acid (iso-Diabolic Acid), a common membrane-spanning lipid of acidobacteria subdivisions 1

and 3. Appl. Environ. Microbiol. 77, 4147–4154. https://doi.org/10.1128/AEM.00466-11.

Sun, D.H., Bloemendal, J., Yi, Z.Y., Zhu, Y.H., Wang, X., Zhang, Y.B., Li, Z.J., Wang, F., Han, F., Zhang, Y., 2011. Palaeomagnetic and palaeoenvironmental study of two parallel sections of late Cenozoic strata in the central Taklimakan Desert: Implications for the desertification of the Tarim Basin. Palaeogeogr. Palaeocl. 300, 1–10.

Thiel, V., Jenisch, A., Landmann, G., Reimer, A., Michaelis, W., 1997. Unusual distributions of long-chain alkenones and tetrahymenol from the highly alkaline Lake Van, Turkey. Geochim. Cosmochim. Acta 61, 2053–2064.

Tierney, J.E., Russell, J.M., 2009. Distributions of branched GDGT in a tropical lake system: Implications for lacustrine application of the MBT/CBT paleoproxy. Org. Geochem. 40, 1032–1036.

van Baak, C.G.C., Vasiliev, I., Stoica, M., Kuiper, K.F., Forte, A.M., Aliyeva, E., Krijgsman, W., 2013. A magnetostratigraphic time frame for Plio-Pleistocene transgressions in the South Caspian Basin, Azerbaijan. Glob. Planet. Chang. 103, 119–134.

van Baak, C.G.C., Grothe, A., Richards, K., Stoica, M., Aliyeva, E., Davies, G., Kuiper, K. F., Krijgsman, W., 2019. Flooding of the Caspian Sea at the intensification of Northern Hemisphere Glaciations. Glob. Planet. Chang. 174, 153–163.

van der Meer, M.T.J., Sangiorgi, F., Baas, M., Brinkhuis, H., Sinninghe Damsté, J.S., Schouten, S., 2008. Molecular isotopic and dinoflagellate evidence for late Holocene freshening of the Black Sea. Earth Planet. Sci. Lett. 267, 426–434.

Vasiliev, I., Reichart, G.J., Krijgsman, W., 2013. Impact of the Messinian Salinity Crisis on Black Sea hydrology-Insights from hydrogen isotopes analysis on biomarkers. Earth Planet. Sci. Lett. 362, 272–282.

Vasiliev, I., Reichart, G.J., Grothe, A., Sinninghe Damsté, J., Krijgsman, W., Sangiorgi, F., Weijers, J.W.H., van Roij, L., 2015. Recurrent phases of drought in the upper Miocene of the Black Sea region. Palaeogeogr. Palaeoclimatol. Palaeoecol. 423, 18–31.

Vasiliev, I., Reichart, G.J., Krijgsman, W., Mulch, A., 2019. Black Sea rivers capture drastic change in catchment-wide mean annual temperature and soil pH during the Miocene-to-Pliocene transition. Glob. Planet. Chang. 172, 428–439.

Vasiliev, I., Feurdean, A., Reichart, G.J., Mulch, A., 2020. Late Miocene intensification of continentality in the Black Sea region. Int. J. Earth Sci. 109, 831–842.

Vincent, S.J., Davies, C.E., Richards, K., Aliyeva, E., 2010. Contrasting Pliocene fluvial depositional systems within the rapidly subsiding South Caspian Basin; a case study of the palaeo-Volga and palaeo-Kura river systems in the Surakhany Suite, Upper Productive Series, onshore Azerbaijan. Mar. Pet. Geol. 27 (10), 2079–2106. https://doi.org/10.1016/j.marpetgeo.2010.09.007.

Volkman, J.K., Eglinton, G., Corner, E.D.S., Forsberg, T.E.V., 1980. Long chain alkenes and alkenones in the marine coccolithophorid *Emiliania huxleyi*. Phytochemistry 19, 2619–2622.

Weber, L., Moros, M., Weber, Y., Sinninghe Damsté, J.S., 2018. Org. Geochem. 121, 138–154. https://doi.org/10.1016/j.orggeochem.2018.03.007.

Weijers, J.W.H., Schouten, S., Spaargaren, O.C., Sinninghe Damsté, J.S., 2006. Occurrence and distribution of tetraether membrane lipids in soils: Implications for the use of the TEX_{86} proxy and the BIT index. Org. Geochem. 37, 1680–1693. https://doi.org/10.1016/j.orggeochem.2006.07.018.

Weijers, J.W.H., Schouten, S., van der Donker, J., Hopmans, E.C., Sinninghe Damsté, J.S., 2007a. Environmental controls on bacterial tetraether membrane lipid distribution in soils. Geochim. Cosmochim. Acta 71, 703–713.

Weijers, J.W.H., Schouten, S., Sluijs, A., Brinkhuis, H., Sinninghe Damsté, J.S., 2007b. Warm arctic continents during the Palaeocene–Eocene thermal maximum. Earth Planet. Sci. Lett. 261, 230–238.

Weiss, G., Schouten, S., Sinninghe-Damsté, J.S., van der Meer, M.T.J., 2019. Constraining the application of hydrogen isotopic composition of alkenones as a salinity proxy using marine surface sediments. Geochim. Cosmochim. Acta 250, 34–48.

Yanchilina, A.G., Ryan, W.B.F., Kenna, T.K., McManus, J.F., 2019. Meltwater floods into the Black Sea and Caspian Sea during Heinrich Stadial 1. Earth Sci. Rev. 198, 102931.

Yanina, T.A., 2013. Biostratigraphy of the middle and upper Pleistocene of the Caspian region. Quat. Int. 284 https://doi.org/10.1016/j.quaint.2012.02.008, 85e97.

Zhang, Z., Ramstein, G., Schustre, M., Li, C., Contoux, C., Yan, Q., 2014. Aridification of the Sahara desert caused by Tethys Sea shrinkage during the late Miocene. Nature 513, 401.

Zhu, C., Weijers, J.W.H., Wagner, T.J., Pan, M., Chen, J.F., Pancost, R.D., 2011. Sources and distributions of tetraether lipids in surface sediments across a large river-dominated continental margin. Org. Geochem. 42, 376–386. https://doi.org/10.1016/j.orggeochem.2011.02.002.

Zonn, I.S., Kosarev, A.N., Glantz, M., Kostianoy, A.G., 2010. The Caspian Sea, Encyclopedia. Springer, Berlin, Heidelberg. https://doi.org/10.1007/978-3-642-11524-0. XI, 525pp, ISBN 978–3–642-11524-0.